AD-A274 376

TION PAGE

Form Approved
OMB No. 0704-0188

1. AGENCY USE ONLY (Leave blank)	2. REPORT DATE	3. REPORT TYPE AND DATES COVERED
		Final Report 01 Oct 92 - 30 Sep 93

4. TITLE AND SUBTITLE
Experiments and Numerical Simulations of Electromagetic Wave Propagation in Plasma Varying Rapidly in Space and Time

5. FUNDING NUMBERS
AFOSR-91-0002

(2)

6. AUTHOR(S)
Professor S. P. Kuo

7. PERFORMING ORGANIZATION NAME(S) AND ADDRESS(ES)
Polytechnic University
Department of Electrical Engineering
Brooklyn NY 11201

AFOSR-TR-

8. PERFORMING ORGANIZATION REPORT NUMBER

9. SPONSORING/MONITORING AGENCY NAME(S) AND ADDRESS(ES)
AFOSR/NE
110 Duncan Avenue Suite B115
Bolling AFB DC 20332-0001

10. SPONSORING/MONITORING AGENCY REPORT NUMBER
2301/ES

11. SUPPLEMENTARY NOTES

12a. DISTRIBUTION/AVAILABILITY STATEMENT
UNLIMITED

This document has been approved for public release and sale; its distribution is unlimited.

12b. DISTRIBUTION CODE

13. ABSTRACT (Maximum 200 words)

SEE PAGE 1 FOR INTRODUCTION

14. SUBJECT TERMS	15. NUMBER OF PAGES
	83
	16. PRICE CODE

17. SECURITY CLASSIFICATION OF REPORT	18. SECURITY CLASSIFICATION OF THIS PAGE	19. SECURITY CLASSIFICATION OF ABSTRACT	20. LIMITATION OF ABSTRACT
UNCLASS	UNCLASS	UNCLASS	UL

Polytechnic UNIVERSITY

Technical Annual Report to
Air Force Office of Scientific Research
Grant AFOSR-91-0002

(October 1, 1992 - September 30, 1993)

Experiments and Numerical Simulations of Electromagnetic Wave Propagation in Plasma Varying Rapidly in Space and Time

Submitted by

A. Ren

S. P. Kuo, Principal Investigator

ACKNOWLEDGMENT:

The work presented in this report is taken from the Ph.D. dissertation of A. Ren who has been supported by the research fellowship through the AFOSR Grant during the past 5 years.

A. Ren would like to acknowledge the funding support of the U. S. Air Force that enabled him to complete the Ph.D. degree requirements at the Polytechnic University and in particular to thank Dr. Robert Barker, the program manager of the AFOSR Grant, for his encouragement and interest in the research work presented in this report.

Table of Contents

Chapter I

Introduction

The propagation of an electromagnetic wave through plasma medium has been studied for a long time. Various processes have been explored. One of them, as the dispersive property of the plasma medium, is the cutoff of the wave propagation when the plasma frequency of an unmagnetized plasma becomes higher than the wave frequency. In a time varying plasma, its modification to the wave propagation is even more dynamical. It has been shown that the interaction between an electromagnetic wave and a fast growing plasma can lead to the spectral change of the original wave. As early as 1973, Yablonovitch[1,2] demonstrated that the frequencies of the output pulses were up-shifted and down-shifted in the experiments of gas breakdown by high power CO_2-laser pulses. In 1975 Jiang[3] analyzed the problem using Laplace transformation. The result showed that a microwave pulse propagating in a time switch medium could be broken up into two propagating parts together with a non-propagating static magnetic field part. The propagating parts consisted of a forward and a backward wave. The carrier frequencies of both propagating components were changed. But only recently, a comprehensive theory and numerical simulation on this subject was presented by Wilks et al.[4]. Their work stimulated a renewed interest in this subject and several new experiments followed.

One of them conducted by our group[5] was performed by using two crossed beam microwave pulses for plasma generation in their intersection region inside a Plexiglas chamber of 2 foot cube. The frequency spectrum of the same pulses at the exit side of the chamber were examined. The results showed that central frequencies of the transmitted pulses were up-shifted. Moreover, the shapes of the transmitted pulses were shown to experience very little distortion. The percentage of frequency shift was found to be consistent with the theory of Wilks et al. Other demonstrations of frequency up-shifting of microwave by rapid plasma creation were conducted by experiments of Joshi et al[6] and Rader et al.[7] The experiment of Joshi et al was carried out in a cavity in which the

plasma was rapidly created by ionizing the background azulene vapor with a laser pulse. The frequency of the incident RF wave at 33.3 GHz was up-shifted by 5% with greater than 10% of efficiency. Signals with much higher up-shifted frequencies were also observed. Their generation mechanism was later confirmed experimentally by Savage et al[8] to be associated with the relativistic Doppler shift effect. The experiment of Rader et al was performed in a long cylindrical tube in which the plasma was generated by a DC discharge and the source wave of 2.68 GHz was passed through and reflected back from the other end. A 0.2% up-shift from the source wave frequency was reported.

The physical mechanism underlying the phenomenon of emerging new waves with up-shifted frequencies is based upon the phase velocity transitions. In plasma medium, the phase velocity of an electromagnetic wave increases with the plasma density. However, it is noted that the wavelength $\lambda_0=2\pi/k_0$ of the wave does not change after a sudden increase of the plasma density. This is due to the wave experiences only the temporal variation of the plasma medium. The sudden reduction of the index of reflection of the plasma, from the initial value $\varepsilon_r=1-\omega_{pe0}^2/\omega_0^2\approx 1$ to a new one $\varepsilon_r=1-\omega_{pe}^2/\omega^2$ resulting from conversion of the background gas into a dense plasma having a plasma frequency ω_{pe}, is going to force the wave to propagate with a faster phase velocity. Thus, the new wave has to oscillate with higher angular frequency $\omega=(\omega_0^2+\omega_{pe}^2)^{1/2}$ at subsequent time, in order to satisfy the dispersion relation $\varepsilon_r=k_0^2c^2/\omega^2$.

The result of frequency conversion has various potential applications. It can provide variable frequency bandwidth for a coherent source whose frequency tuning capability can thus be improved. Such a wideband coherent source can be used in spectroscopy, radar, chemistry, medical imaging and plasma diagnostics. Presently, any one such device is only tunable over a limited frequency range. The plasma introduced frequency conversion process has the potential to extend the usage of an existing coherent source, and therefore, it is of great interest to explore the feasibility of a practical device based on such a process. The plasma introduced frequency conversion process also makes

it possible to chop a CW wave into an ultra-wideband pulse train[9,10]. To achieve this, a periodic discharge of gas is required and the pattern of the pulse train depends on the temporal pattern of the plasma density of gaseous discharge. The frequency conversion process may be used to devise a plasma cloaking system which alters the radar signal frequency so that the return signal is out of the receiving band of the radar system, and the target becomes effectively radar invisible[11].

Moreover, in using high power microwave pulses for the applications of radar and directed energy systems, it is crucial to identify the effect of self-generated plasma on the propagation of the pulses. Since the density of the pulse-generated plasma is a space-time function, it can radically modify wave propagation[12-19]; in particular, a phenomenon called "tail erosion" plays a primary role in limiting the energy transfer of the pulse from the source to the target.[17,18] It was found that most of the pulse's energy was wasted by cutoff reflection and the remaining leading edge of the pulse became too narrow to deliver enough energy for the applications of interest. Therefore, the frequency up-shift effect in a time varying plasma may be a viable mechanism leading to disired reflectionless propagation of very powerful microwave pulses through the air. Gildenburg et al.[20] showed that, under the condition that the ionization frequency of the background gas is much larger than the collision frequency of electrons, the carrier frequency ω of the pulse indeed shifts upward to keep $\omega > \omega_{pe}$ during the growth of the plasma density, where ω_{pe} is the electron plasma frequency. Hence, the self-generated plasma will always be underdense to the pulse through this frequency auto-conversion process[21,22].

The plasma media which may result frequency conversion to the propagating wave can be classified into two categories:

1) plasma density varies temporally together with spatial variation, such as the self-generated plasma along the trail of a high power microwave pulse.

2) plasma density varies only temporally (spatially uniform over several wavelengths.), such as a plasma created suddenly by a DC glow discharge between two parallel plate electrodes.

The wave propagation through ionizable medium in either category should be considered as an initial value problem, though the boundary effects have also to be included in the analysis. Therefore, the spectral change of the original electromagnetic wave is expected in both cases. Moreover, the frequency shift can contain both up and down components. The plasma decay rate is usually too slow to account for frequency down shift effect, however, the loss rate of the wave in plasma can be quite large and introduces significant frequency down shift effect.

This dissertation is organized as follows: Chapter II presents the study on the frequency conversion of high power microwave pulse propagating through a self-generated plasma, which falls into the first category. In section 1, a theoretical model is developed and discussed. A chamber experiment is conducted to demonstrate the frequency up-shift phenomenonin. The results are presented in section 2, which is followed in section 3 by the numerical simulation of the experiment. In section 4, experiments with higher microwave power are performed and give results revealing both frequency up-shift and down-shift in the form of spectral breaking. The numerical simulations are also performed to get better understanding of the experimental results. Section 5 presents a series of computer experiments performed to identify that the collision loss of the wave in the plasma is the cause of frequency down-shift process which leads to spectral breaking. Section 6 of the chapter gives a summary of the study. The study on the subject of up-shifting a CW wave propagating through a rapidly created plasma is presented in Chapter III. The plasma involved in this case falls into the second category. Again, a theoretical model is first developed and discussed in section 1. Then, experiments for two cases distincted by the maximum plasma frequency is smaller or larger than the wave frequency are reported in section 2A and section 2B respectively. In

section 3 the numerical simulations of the conducted experiments are reported. A summary of the work is presented in section 4. Finally, in chapter IV, a conclusion of the research efforts is drawn.

Chapter II

Frequency Conversion of a High Power Microwave Pulse Propagating in a Self-generated Plasma

High power electromagnetic wave propagating through a gaseous medium can cause the background gas breakdown and form a space-time dependent plasma along the trail of its propagation path. Thus, the wave is unavoidable to interact with a self-generated plasma which can radically modify the wave propagation. High power radar and directed energy systems encounter this problem. The spectral variation of the forward scattered wave propagating in such a plasma environment is of the interest of this chapter.

1. Theoretical Model

Consider an electromagnetic pulse propagating in an ionizable medium (gas) and the pulse is intense enough to break down the background gaseous medium. Thus, the plasma is generated by the powerful microwave pulse along the trail of the pulse. The density of the electron plasma is a space-time function and is strongly dependent on the intensity, width, and the shape of the pulse as well as the loss processes in the background medium, which include attachment, recombination, and diffusion. Hence, during the microwave pulse ionizing period, the rate equation for electron plasma density n_e is given by

$$\frac{\partial}{\partial t} n_e = (\nu_i - \nu_a) n_e - \gamma n_e^2 \qquad (1)$$

where ν_i, ν_a, and γ, are the ionization frequency, attachment frequency, and recombination coefficient, respectively. The diffusion term is neglected. Since the time scale considered is much faster than the time for diffusion to take place. The ionization frequency is modeled as[23]:

$$\nu_i=3.83\times10^2\nu_a[\varepsilon^{3/2}+3.94\varepsilon^{1/2}]\exp[-7.546/\varepsilon] \qquad (2)$$

where $\varepsilon=|A/A_{th}|$ is the wave field amplitude A normalized to the breakdown (ionization) threshold field amplitude A_{th} ; $A_{th}\sim18p(1+\omega^2/\nu^2)^{1/2}$ V/cm for continuous wave in which p is the background pressure in torr[24].

The electron momentum equation including the momentum loss due to both elastic and inelastic collision is

$$\frac{\partial}{\partial t}(n_e\bar{v}_e)=-n_e e\bar{E}/m_e-(\nu+\nu_a+\gamma n_e^2+\eta\nu_i)n_e\bar{v}_e \qquad (3)$$

where $\eta=(\varepsilon_i/KE)^{1/2}$, the square root of the ratio of the ionization energy ε_i of the background gas to the electron average kinetic energy KE, gives a measure of effective momentum loss in each ionization event.

From Maxwell equations, one has wave equation

$$\frac{\partial^2}{\partial t^2}\bar{E}-c^2\frac{\partial^2}{\partial z^2}\bar{E}=-4\pi\frac{\partial}{\partial t}\bar{J} \qquad (4)$$

where $\bar{J}=-en_e\bar{v}_e$. Using (3), equation (4) becomes

$$\frac{\partial^2}{\partial t^2}\vec{E}-c^2\frac{\partial^2}{\partial z^2}\vec{E}+\omega_{pe}^2\vec{E}=-\omega_{pe}^2(m_e/e)\nu_1\vec{v}_e \qquad (5)$$

where $\nu_1=\nu+\nu_a+\gamma n_e^2+\eta\nu_i$. With the aid of (1), (3) can be reduced to

$$\frac{\partial}{\partial t}\vec{v}_e=-e\vec{E}/m_e-[\nu+(\eta+1)\nu_i]\vec{v}_e=-e\vec{E}/m_e-\nu_2\vec{v}_e \qquad (6)$$

where $\nu_2=\nu+(\eta+1)\nu_i$.

Assume that the expression for $\vec{E}$ is $\vec{E}(z,t)=\hat{x}A(z,t)\exp[-i\phi(z,t)]+$c.c. for real A and ϕ with c.c. representing the complex conjugate. If the pulse is not too short, i.e. it carries many oscillations, then the variation of the amplitude function A(z,t) in space and time is slower than that of the phase function $\exp[-i\phi(z,t)]$. It is also true to the corresponding velocity response which is expressed accordingly as $\vec{v}_e(z,t)=\hat{x}V(z,t)\exp[-i\phi(z,t)]+$c.c.. Hence, $|\partial lnA/\partial t|$ and $|\partial lnV/\partial t| << |\partial\phi/\partial t|$ and $|\partial lnA/\partial z|$ and $|\partial lnV/\partial z| << |\partial\phi/\partial z|$ which will be employed in the analysis. In addition. the forward-scattering approximation leading to the definition of local frequency $\omega=\partial\phi/\partial t$ and local wave number $k=-\partial\phi/\partial z$ will also be used to simplify the analysis. This approximation is justified because only the portion of the pulse propagating in the forward direction is of interest.

Using these approximations, and the relationship $V(z,t)=-ieA(z,t)/m_e(\omega+i\nu_2)$ obtained from (6), (5) leads to

$$\frac{\partial^2}{\partial t^2}\vec{E}-c^2\frac{\partial^2}{\partial z^2}\vec{E}+\omega_{pe}^2\vec{E}=i\omega_{pe}^2\nu_1\vec{E}/(\omega+i\nu_2)$$

which can be rewritten as:

$$(\frac{\partial^2}{\partial t^2}-c^2\frac{\partial^2}{\partial z^2}+\omega_{pe}^2)\bar{E}=[\omega_{pe}^2\nu_1\nu_2/(\omega^2+\nu_2^2)+i\omega_{pe}^2\nu_1\omega/(\omega^2+\nu_2^2)]\bar{E} \qquad (7)$$

Taking the scalar product of $\bar{E}^*$ and (7), and neglecting the two high order terms $A\frac{\partial^2}{\partial t^2}A$ and $c^2A\frac{\partial^2}{\partial z^2}A$, yield

$$\omega^2-k^2c^2=\omega_{pe}^2[1-\nu_1\nu_2/(\omega^2+\nu_2^2)] \qquad (8)$$

and

$$\frac{\partial}{\partial t}(\omega A^2)+\frac{\partial}{\partial z}(kc^2A^2)=-[\omega_{pe}^2\nu_1\omega/(\omega^2+\nu_2^2)]A^2 \qquad (9)$$

Equation (8) is the local dispersion relation of the wave, and equation (9) is the continuity equation for the energy density of the pulse. From their definitions, ω and k are related by the equation $\frac{\partial}{\partial t}k+\frac{\partial}{\partial z}\omega=0$.

Using (8), (9) is expressed as

$$\frac{\partial}{\partial t}P+\frac{\partial}{\partial z}\{c\{1-[\omega_{pe}^2/\omega^2][1-\nu_1\nu_2/(\omega^2+\nu_2^2)]\}^{1/2}P\}=-[\omega_{pe}^2\nu_1/(\omega^2+\nu_2^2)]P \qquad (10)$$

where $P=\omega A^2$ is proportional to the energy density of the microwave pulse.

The phase velocity and the group velocity of the wave in a self-generated plasma can be derived as:

$$v_p=\omega/k=c/\{1-[\omega_{pe}^2/\omega^2][1-\nu_1\nu_2/(\omega^2+\nu_2^2)]\}^{1/2} \qquad (11)$$

and

$$v_g=\frac{\partial}{\partial k}\omega=c\{1-[\omega_{pe}^2/\omega^2][1-\nu_1\nu_2/(\omega^2+\nu_2^2)]\}^{1/2}/[1-\omega_{pe}^2\nu_1\nu_2/(\omega^2+\nu_2^2)^2] \qquad (12)$$

From equation (11) one can see it clearly that the higher the plasma frequency (plasma density), the higher the phase velocity of the wave. On the other hand, the phase velocity of the wave decreases as the term $\nu_1\nu_2/(\omega^2+\nu_2^2)$ increases (i.e. the loss increases). Since the phase velocity of the wave may decrease when there is loss, the frequency down-shift is also possible. It is also noticed from equation (12) that the group velocity of the wave decreases with the plasma frequency. When the plasma frequency ω_{pe} increases to the value about $(\omega^2+\nu_1\nu_2)^{1/2}$, the group velocity of the wave reduces to zero, i.e., the wave is cutoff from the propagation by the plasma.

Taking the time derivative of (8) and using the relation $\frac{\partial}{\partial t}k+\frac{\partial}{\partial z}\omega=0$ and (12), it leads to

$$\frac{\partial}{\partial t}\omega^2+v_g\frac{\partial}{\partial z}\omega^2=\{[1-\nu_1\nu_2/(\omega^2+\nu_2^2)]/[1-\omega_{pe}^2\nu_1\nu_2/(\omega^2+\nu_2^2)^2]\}\frac{\partial}{\partial t}\omega_{pe}^2 \qquad (13)$$

Equations (1), (10) and (13) together with (2) and (12) form a complete set of modal equations describing the dynamic of pulse propagation in the self-generated plasma. The local wave number and phase velocity of the wave can then be obtained from (8) and (11).

In terms of total time derivative, i.e. $\frac{d}{dt}=\frac{\partial}{\partial t}+v_g\frac{\partial}{\partial z}$, (13) can be rewritten as:

$$\frac{d}{dt}(\omega^2-\omega_{pe}^2)=-\{[\nu_1\nu_2/(\omega^2+\nu_2^2)][1-\omega_{pe}^2/(\omega^2+\nu_2^2)]/[1-\omega_{pe}^2\nu_1\nu_2/(\omega^2+\nu_2^2)^2]\}\frac{\partial}{\partial t}\omega_{pe}^2$$

$$-v_g\frac{\partial}{\partial z}\omega_{pe}^2 \qquad (14)$$

In the case of $\nu_1\nu_2/(\omega^2+\nu_2^2)<<1$, the first term on the right-hand side of (14) is negligible, and (14) is reduced to

$$\frac{d}{dt}(\omega^2-\omega_{pe}^2)=-v_g\frac{\partial}{\partial z}\omega_{pe}^2 \qquad (15)$$

Considering a rectangular pulse whose envelop is shown in Fig. 1, the density of the generated plasma at a given time is expected to grow nearly exponentially from the background level at the leading edge of the pulse to a peak at the tail end of the pulse. Behind the pulse, plasma density drops from its peak value at a rate depending on the loss mechanisms. The envisioned density profile is also plotted in Fig. 1. It is shown that $\frac{\partial}{\partial z}\omega_{pe}^2\le 0$ in the pulse interval and consequently, $\frac{d}{dt}(\omega^2-\omega_{pe}^2)>0$, which means $(\omega^2-\omega_{pe}^2)$ increases in time. Thus, as long as $\omega>\omega_{pe}$ initially, which is true because the background has very low plasma density, ω will remain greater than ω_{pe} as the microwave pulse propagates. In other words, the carrier frequency of the microwave pulse is up-shifted and remains greater than the plasma frequency while the plasma density increases because of the gas breakdown. This frequency up-shift process leads to the reflectionless (without cutoff reflection) propagation of a high power microwave pulse in a self-generated plasma. This conclusion seems trivial for a rectangular pulse propagating in a uniform medium because $\frac{d}{dt}\omega_{pe}^2<0$. However, it becomes a significant result for pulse propagating in a non-uniform medium so that $\frac{d}{dt}\omega_{pe}^2>0$ can occur. An example of this case is the propagation of a pulse through the atmosphere. It is first noted that the breakdown threshold of the air decreases with the altitude before reaching the altitude having a minimum breakdown threshold field. The appearance of such a minimum, similar to the Paschen minimum, can be explained as the result of breakdown by a short pulse that

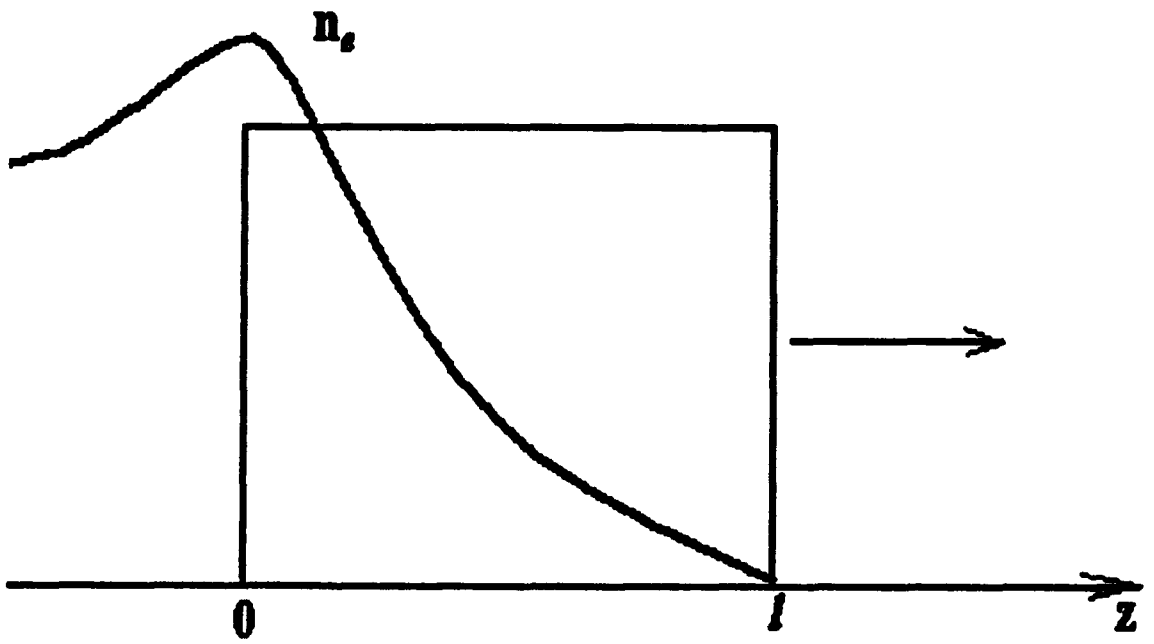

Fig. 1 Envelope of a rectangular pulse and the pulse generated electron plasma density distribution

is equivalent to DC discharge with a short separation gap between electrodes (i.e., short electron transit time). The pulsed nature of the breakdown field also increases the level of the breakdown threshold because the available ionization time at any point along the trail of the pulse is finite and governed by the pulse duration. Beyond that altitude, the breakdown threshold starts to increase with the altitude. Thus, if the pulse is transmitted from the ground to the space, ω_{pe}^2 may increase continuously along the trail of the pulse and exceed $\omega_0^2=\omega^2(t=0,z=0)$ before reaching the altitude of breakdown minimum. However, there is no cutoff reflection throughout the propagation, if $\omega>\omega_{pe}$ initially. Physically, this frequency up-shifting phenomenon can be explained by the fact that the phase velocity of the wave increases with the plasma density. The relationship between phase velocity and plasma density is given by (11). Since the tail part of the pulse experiences higher density than the leading part of the pulse, the tail part propagates faster than the leading part (in terms the phase velocity of the wave), the pulse is squeezed toward its front as time evolves. Consequently, the wave frequency is up-shifted. It is noted that such a frequency auto conversion process is also helping the pulse propagating from space to the ground since the breakdown threshold again decreases with the propagation distance before passing through the breakdown minimum.

The amount of frequency up-shift during the propagation can also be estimated from (14) which is rewritten, with the aid of (1), as

$$\frac{d}{dt}\omega^2=\frac{\partial}{\partial t}\omega_{pe}^2=(\nu_i-\nu_a)\omega_{pe}^2 \qquad (14')$$

where the recombination loss is neglected.

Approximate $(\nu_i-\nu_a)$ by $ln(n_e/n_0)/\tau$, the average increase rate of the electron plasma density, where τ is the ionizing period, and n_0 is the background electron plasma density, and replace dt by $dz/v_g \sim dz/[c(1-n_e/n_c)^{1/2}]$, where n_c is the cutoff density of the

self-generated plasma. Equation (14') can be integrated along the trajectory of the pulse z to obtain

$$\Delta f=(f_0/2c\tau)\int_0^L dz(n_e/n_c)/n(n_e/n_0)/(1-n_e/n_c)^{1/2} \qquad (16)$$

where $\omega_{pe}^2/\omega_0^2=n_e/n_c$ is employed.

For the situation that $\nu_1\nu_2/(\omega^2+\nu_2^2)<<1$ does not hold, one can show that the frequency down-shift may occur. Let the effective loss $\nu_1\nu_2/(\omega^2+\nu_2^2)=\bar{\nu}$, the relative electron plasma density $\omega_{pe}^2/(\omega^2+\nu_2^2)=n_e/n_c=n$, where n_c is the cutoff plasma density for the wave. Equation (14) reduces to

$$\frac{d}{dt}(\omega^2-\omega_{pe}^2)=-\bar{\nu}[(1-n)/(1-\bar{\nu}n)]\frac{\partial}{\partial t}\omega_{pe}^2-v_g\frac{\partial}{\partial z}\omega_{pe}^2 \qquad (15')$$

where $\bar{\nu}$ and n are both less than 1, and $\frac{\partial}{\partial t}\omega_{pe}^2\geq 0$ in most of the situations as the pulse is intensive enough to break down the gas. However, if the tail erosion is severe and the plasma loss is high, $\frac{\partial}{\partial t}\omega_{pe}^2$ may be less than zero. The first term in the right hand side of equation (15') has the opposite sign with $\frac{\partial}{\partial t}\omega_{pe}^2$, hence, when $\frac{\partial}{\partial t}\omega_{pe}^2>0$ and $\left|\bar{\nu}[(1-n)/(1-\bar{\nu}n)]\frac{\partial}{\partial t}\omega_{pe}^2\right|>\left|v_g\frac{\partial}{\partial z}\omega_{pe}^2\right|$, $\frac{d}{dt}(\omega^2-\omega_{pe}^2)<0$, the wave frequency is down-shifted. Therefore, in the case of $\nu_1\nu_2/(\omega^2+\nu_2^2)\sim 1$, the frequency conversion may happen in either way, i.e. up- or down-shift, depending on the $\bar{\nu}$ and n values and if the remaining field intensity is strong enough to continuously break down the background gas. These factors are not independent from each other. The $\bar{\nu}$ value depends on collision frequency and other loss processes, as well as the wave frequency. In fact, $\bar{\nu}$ is a measure

of total effective loss rate, and is a function of background gas pressure, pulse intensity, electron plasma density and the wave frequency. The relative electron plasma density n is strongly dependent on the intensity, width, the shape of the pulse, the background gas breakdown threshold and the loss processes. Hence, the frequency conversion is actually related to the value of collision frequency and the ratio of the pulse intensity to the breakdown threshold intensity of the background gas. Equation (15') suggests that the frequency down-shift will occur when $\overline{\nu}$ is large and the power of the microwave pulse is high. It will be confirmed both experimentally and numerically and presented in section 4. The numerical simulation will be based on the set of equations (1), (10) and (13). In the next section the experiment only on frequency up-shift of a pulse propagating in a self-generated plasma is reported.

2. Experimental demonstrations of Frequency up-conversion

The experiments of pulse propagation are conducted in a vacuum chamber filled with dry air. The chamber is made of a 2 foot cube of Plexiglas with the thickness of one inch. Fig. 2 (a) is a photograph of the chamber. A microwave pulse is fed into the cube through an S-band horn placed at one side of the chamber. A second S-band horn placed at the opposite side of the chamber is used to receive the transmitted pulse. The microwave pulse is generated by a single magnetron tube (OKH 1448) driven by a soft tube modulator. The magnetron produces 1 MW peak output power at a central frequency of 3.27 GHz. The modulator is triggered by a pulse-forming network (PFN) having a pulse width of 1 μs and a repetition rate ranging between 20 and 60 Hz. An HP 8569B spectrum analyzer is used to record the spectra of the incident and the transmitted pulse. The spectra of the incident pulse and transmitted pulse are then compared. The

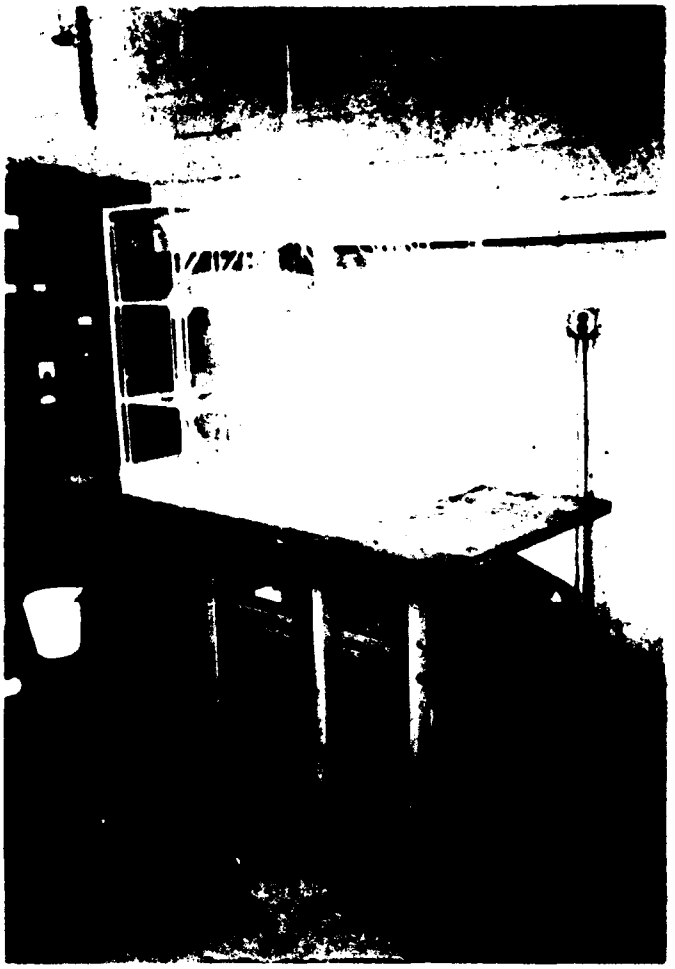

Fig. 2 (a) The Plexiglas chamber

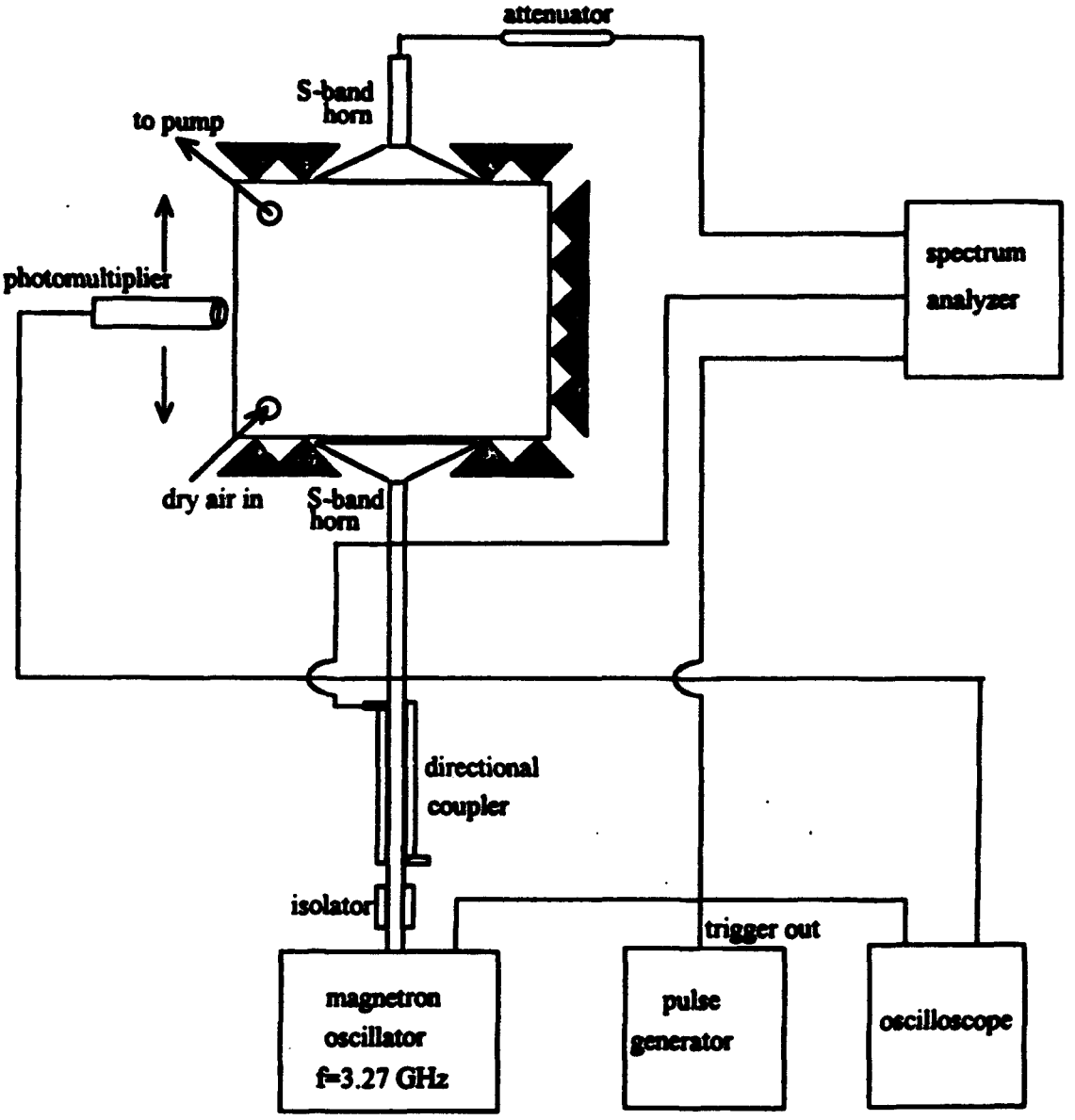

Fig. 2 (b) Experimental setup for the experiment of high power microwave pulse propagating in a self-generated plasma--frequency up-shift.

density profile of the electron plasma along the propagating direction is measured in terms of the enhanced airglow through a photomultiplier.

The block diagram of the experimental setup is shown in Fig. 2 (b). A directional coupler connected to the incident horn is used to monitor the spectrum of the input pulse which is used as a reference. The air pressure in the chamber is about 0.08 torr, and thus, the electron-neutral collision frequency ν is below $5\times10^8\sqrt{T_e}\ s^{-1}$, where T_e is the electron temperature measured in eV. Limited by the available power of the magnetron tube, the ionization frequency ν_i in such a background pressure is less than $10^8 s^{-1}$. ν_a is in the order of 6×10^4/torr by measurement[16]. Since the recombination process is much slower than the ionization process, the γn_e term can be neglected compared to ν. The η coefficient is in the order of 10. Hence, $\nu_1\nu_2 << \omega^2+\nu_2^2$ is justified. The frequency up-shift is expected in the present experiment.

In order to estimate the amount of frequency up-shift, one has to get the electron plasma density profile along the pulse propagation trail. A photomultiplier monitoring the enhanced airglow is used for this purpose. The relationship between the airglow and electron plasma density is calibrated by a Langmuir double probe[25]. Using focusing lenses to localize the enhanced airglow, its temporal evolution at a fixed point on the pulse trail is then recorded on the oscilloscope through the photomultiplier. By moving the optical probe parallel to the path of the pulse, the variation of the peak airglow intensity along the path is determined. Then the absolute value of the electron plasma density can be calibrated by measuring the plasma density with a Langmuir double probe at a point where the airglow intensity is also recorded simultaneously. It is noted that the airglow is generated mainly through impact excitation of neutral gas, which requires that the electron energy exceeds 2eV. From this point of view, the axial distribution of the peak airglow does not actually represent, in general, the axial distribution of the peak plasma density. Nevertheless, it provides a good approximation especially since only the distribution of the peak airglow intensity is considered.

In the present experiment, two different incident power levels are used. $P_1=1.1P_c$ and $P_2=1.3P_c$, where P_c is the power of the pulse causing merely a sign of air breakdown which is indicated either visually, as the first sign of a glow in the chamber, or as the distortion in the shape of the pulse received by the horn placed at the opposite side of the chamber. The experiment shows that these two signs of merely breakdown of the background gas are actually happening simultaneously. Although the differences of these two levels of the incident power seems not to be significant, the results turn out quite differently because the ionization rate is extremely sensitive to the field strength. The corresponding electron plasma density distribution along the propagation path are also measured for the purpose of estimating the amount of frequency up-shift and comparison between the two cases. Fig. 3 (a) and Fig. 4 (a) show the measured density profile along the trail of the transmitted pulse corresponding to the incident power of $1.1P_c$ and $1.3P_c$ respectively. Fig. 3 (b) and Fig. 4 (b) show the recorded spectra of the incident and transmitted pulse for power of $1.1P_c$ and $1.3P_c$ respectively. In the first case, $P_1=1.1P_c$, the peak density distribution of the self-generated plasma is shown in Fig. 3 (a), which shows that the plasma density in this case is peaked at the incident boundary and decays quickly. Observe the second and third peaks in the density profile: first, comparing the distance between the two perturbation peaks (1.8" or 4.57 cm) to the half wavelength ($=3\times10^{10}/3.27\times10^{9}=9.17$ cm, $\lambda/2=4.58$ cm), they are the same within the accuracy of 0.1 mm; second, the peak closer to the exit wall (the third peak) has higher density than the one away from the exit wall (the second peak). Since the reflected-wave from the exit wall and the forward transmitting wave form a non-uniform standing wave (the non-uniformity is caused by the lossy plasma medium, the longer the wave propagates in the lossy plasma, the more energy the wave losses). The above mentioned characteristics evidence that these two peaks are caused by the additive contribution of the reflected-wave field from the chamber wall at the exit side. It is noted that the field amplitude is only slightly greater than the breakdown threshold wave field, and a small additive from the reflected-wave

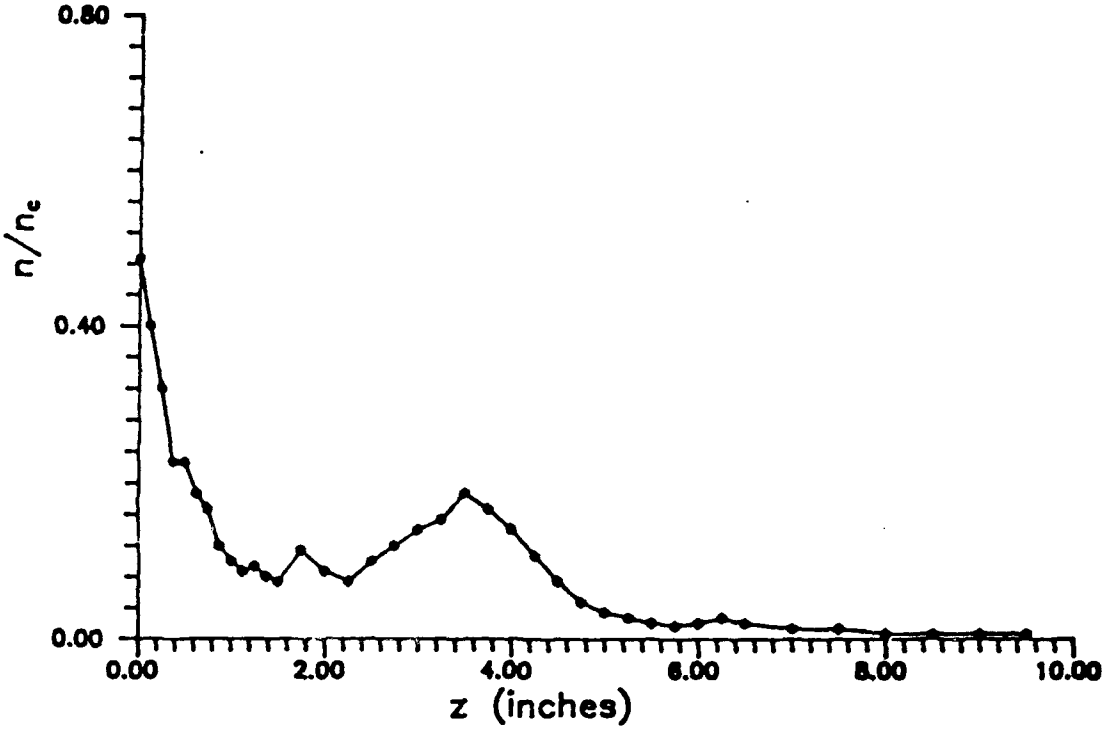

Fig. 3 (a) The measured electron plasma density distribution for $P=1.1P_c$.

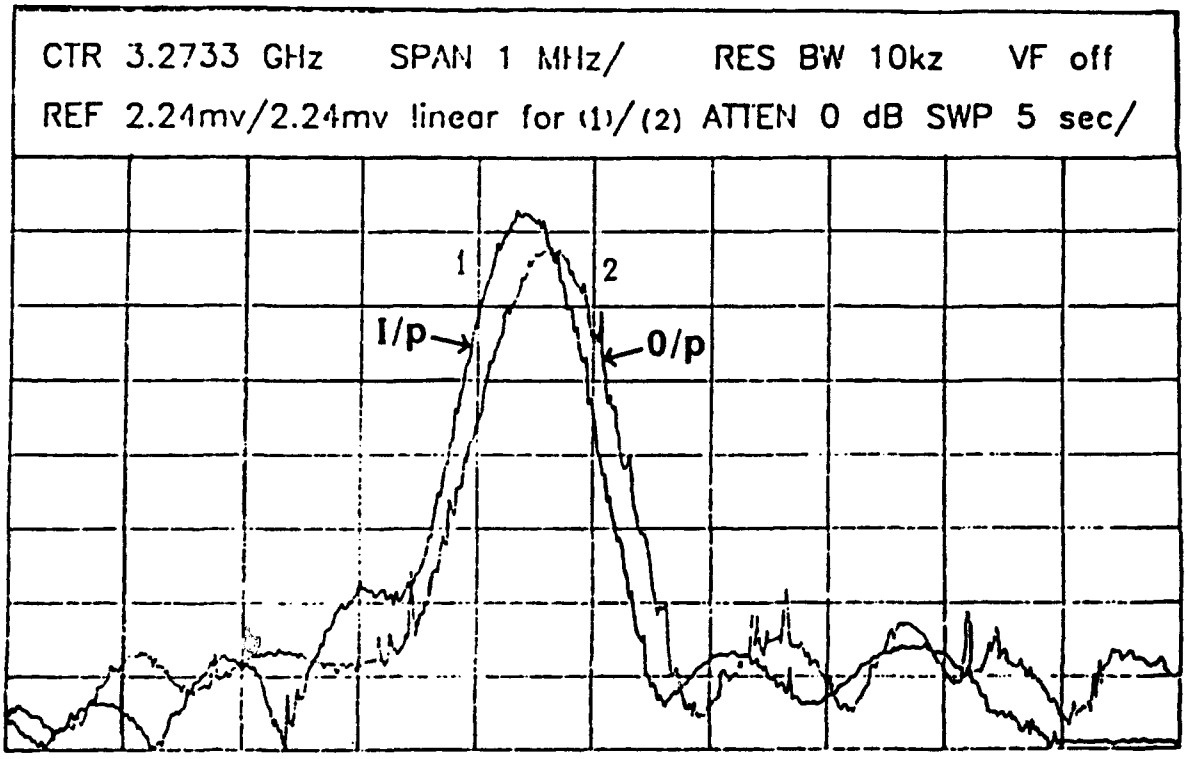

Fig. 3 (b) The recorded spectra of the incident and transmitted pulse for $P=1.1P_c$.

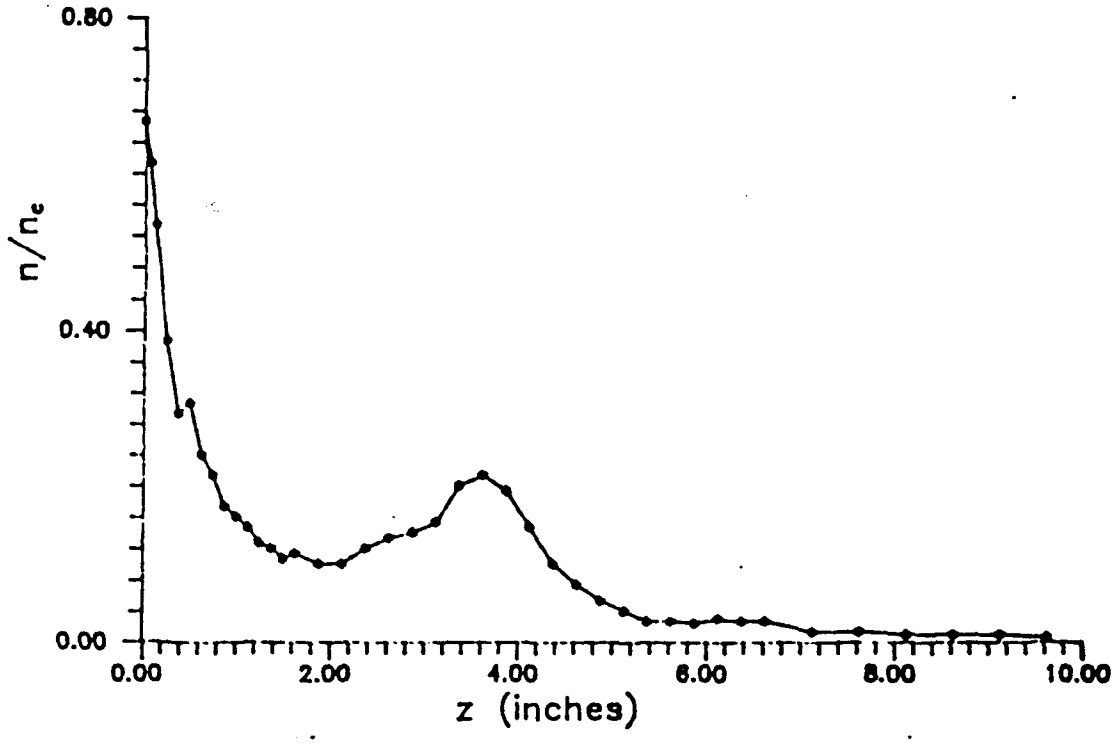

Fig. 4 (a) The measured electron plasma density distribution for $P=1.3P_c$.

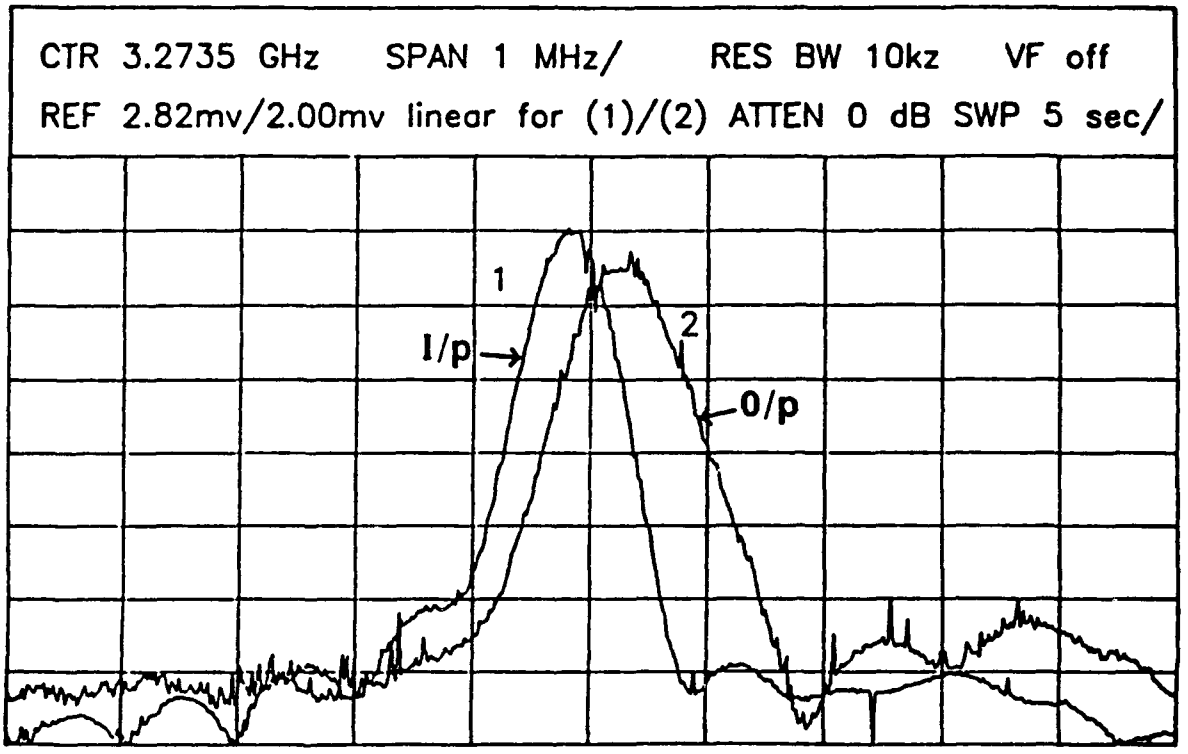

Fig. 4 (b) The recorded spectra of the incident and transmitted pulse for $P=1.3P_c$.

field could result in much larger percentage of density perturbation as shown. This further confirms that the ionization frequency is extremely sensitive to the field strength. The density distribution appears to have a similar decay feature as the expected one presented in Fig. 1. However, the causes of the decay features of the density distribution shown in Fig. 1 and Fig. 3 (a) are quite different. In Fig. 1, the amplitude of the pulse is assumed to be unattenuated (assuming that the amplitude of the pulse well exceeds the breakdown threshold field) and the non-uniformity of the plasma density is due to unequal available ionization time. On the other hand the ionization time at every point in Fig. 3 (a) is about the same because the time required for a wave to travel through the chamber is about 2 ns which is much smaller than the pulse width of 1 μs. However, since the ionization is strongly dependent on the intensity of the wave, the attenuation of the microwave field by the self-generated plasma through the collision and other loss mechanisms have to be taken into account in determining the electron plasma density distribution. Assume that the $<T>=3$ eV, thus, $\nu=8.66\times10^8\ s^{-1}$. Neglect all the other losses (i.e. $\nu_1\approx\nu$, and $\nu_2\approx\nu$), take equation (10), fix the time (i.e. $\frac{\partial}{\partial t}=0$) and integrate along the pulse transmitting path, the energy density of the microwave pulse decays along the path by a factor proportional to

$$\exp\left(-(z/c)[\omega_{pe}^2\nu/(\omega^2+\nu^2)]/\{1-[\omega_{pe}^2/\omega^2][1-\nu^2/(\omega^2+\nu^2)]\}^{1/2}\right)$$

for $\nu^2/\omega^2<<1$ and $<\omega_{pe}^2/\omega^2>\sim1/2$, where $<\ >$ represents the spatial average over the region of interest, the above factor reduces to $\exp(-z\nu/c)$. A quick calculation shows that the energy density $P(=\omega A^2)$ drops to about 93% of the incident value, and wave field A drops to 96.4% of the incident value and the ionization frequency drops to 57% of the maximum value at z=1 inch (2.54 cm) propagation distance, and the electron plasma density drop agrees with the experimental results shown in Fig. 3 (a) and Fig. 4 (a).

Shown in Fig. 3 (b) curve 1 is the frequency spectrum of the input pulse, while curve 2 is the frequency spectrum of the output pulse. The frequency difference between the peaks of these two curves represents the frequency up-shift attributed to the plasma generation in the chamber. Here in Fig. 3 (b) the frequency up-shift is Δf_1=0.26 MHz. The power level P_2=1.3P_c in the second case is chosen for achieving the maximum frequency up-shift without introducing significant distortion to the shape of the pulse. The set of spectra for the input pulse (curve 1) and the output pulse (curve 2) is presented in Fig. 4 (b). The frequency up-shift in this case is Δf_2=0.40 MHz. As shown in Fig. 4 (a), the plasma density in this case is higher than that of the first case shown in Fig. 3 (a).

Using equation (16) and the plasma density profiles presented in Fig. 3 (a) and Fig. 4 (a), the amounts of frequency up-shift are estimated to be Δf_1=0.27 MHz and Δf_2=0.40 MHz, respectively. A good agreement between the results deduced from the theoretical model and the experimental results is clearly shown. To further confirm the theoretical model developed in section 1, numerical simulations of the presented experiments are performed based on the theoretical model and is reported in next section.

3. Numerical simulation

To solve the equation set of (1), (10) and (13), one first normalizes them into dimensionless forms. Using the following definitions: the cutoff plasma density $n_c=(\omega^2 + \nu_2^2)m_e / (4\pi e^2)$, which leads to $n=\omega_{pe}^2/(\omega^2+\nu_2^2)=n_e/n_c$; $\tau=a\omega_0 t \rightarrow t$, where a is a dimensionless constant scaling number to make the time of interest within a convenient number range; $z'=a\omega_0 z/c \rightarrow z$; $\nu_g/c \rightarrow \nu_g$; $\nu_i/\omega_0 \rightarrow \nu_i$; $\nu_a/\omega_0 \rightarrow \nu_a$; $\nu_1/\omega_0 \rightarrow \nu_1$; $\nu_2/\omega_0 \rightarrow \nu_2$; $\omega/\omega_0 \rightarrow \omega$; and $P/P_{th} \rightarrow P$, then equations (1) becomes

$$\frac{\partial}{\partial t}n=(\nu_i-\nu_a)n/a \qquad (17)$$

where the recombination term γn_e^2 has been neglected, and $\frac{\partial}{\partial t}ln[1/(\omega^2+\nu_2^2)]$ is considered much less than $\frac{\partial}{\partial t}ln(n)$ since the density changes much faster than the wave frequency and the collision frequency; and equations (10) and (14) become :

$$\frac{\partial}{\partial t}P+\frac{\partial}{\partial z}\{[1-n(1+\nu_2^2/\omega^2-\nu_1\nu_2/\omega^2)]^{1/2}P\}=-n\nu_1P/a \qquad (18)$$

and

$$\frac{\partial}{\partial t}\omega^2+v_g\frac{\partial}{\partial z}\omega^2=\{[1-\nu_1\nu_2/(\omega^2+\nu_2^2)]/[1-n\nu_1\nu_2/(\omega^2+\nu_2^2)]\}\frac{\partial}{\partial t}n \qquad (19)$$

The equation (14) for the group velocity is also normalized to

$$v_g=[1-n(1+\nu_2^2/\omega^2-\nu_1\nu_2/\omega^2)]^{1/2}/[1-n\nu_1\nu_2/(\omega^2+\nu_2^2)] \qquad (20)$$

Equations (17), (18) and (19) together with (2) and (20) describe the microwave pulse propagating in a self-generated plasma in terms of the dimensionless variables n, P and ω. The normalized initial and boundary conditions are set to be:

$$n(z,t=0)=n_0 \qquad (21)$$

$$P(z=0,t)=P_0\exp\{-[(t-t_0)/t_0]^{10}\}\exp[0.3\sin(t/t_0+0.35)] \qquad (22)$$

$$\omega(z=0,t)=1 \quad , \quad \omega(z,t=0)=1 \qquad (23)$$

where n_0 is the background electron plasma density, P_0 is the power intensity of the pulse, $2t_0$ is the pulse width and $\exp\{-[(t-t_0)/t_0]^{10}\}$ is used to model the rectangular pulse. The electron plasma density n is initially n_0 everywhere, and n is governed by equation (17) which is coupled to (18) through ν_i. Since in the experiment, the envelope of the microwave pulse has some wiggles on top of the rectangular pulse, a factor of $\exp[0.3\sin(t/t_0+0.35)]$ is multiplied to the rectangular pulse as the boundary condition of the power intensity given by equation (22). At the incident boundary $z=0$, P varies in time a pulse with the width of $2t_0$, and at the initial time $t=0$, the front of the pulse is just about to propagate into the chamber. Fig. 5 shows the initial and boundary conditions of power intensity. The frequency ω is 1 at the incident boundary $z=0$ and at the initial time $t=0$, and is governed by equation (19) as time evolves.

A numerical program using the LSODE software package[26-28] is developed for solving the set of equations with the initial and boundary conditions (21), (22) and (23). The parameters are chosen to correspond to those of the experiment, i.e., $t_0=0.5\mu s \rightarrow 0.5a\omega_0$, $\nu_a=6\times10^4/\omega_0$, $n_0=10^{-5}$, $\nu=10\nu_0(P+0.03)^{1/2}$, $\nu_0=3.99\times10^9 p/\omega_0$ with the zero ionization power intensity, where p is the background pressure in torr and p=0.08 torr in the experiment, and $\varepsilon=\sqrt{\frac{P}{\omega}+(\frac{\omega^2}{2\nu_0^2})^2}-\frac{\omega^2}{2\nu_0^2}$. The numerical simulation is performed for two incident power levels, P=1.1 and P=1.3.

Fig. 6 (a) shows the spectra of incident pulse and transmitted pulse for incident power $P=1.1P_c$, which are obtained by taking the Fourier transformation of the transmitted pulse. One can see that the frequency is up-shifted by 0.28 MHz, which is in good agreement with the experiment. Shown in Fig. 6 (b) is the electron plasma density profile as a function of space and time. The maximum density (with respect to time) distribution agrees with the measured maximum density distribution along the pulse trail (Fig. 3 (a)) except for the two perturbation peaks which are found to be contributed by the reflected

pulse from the exit side of the chamber wall. Since the set of equations does not include the effect of the reflected wave from the exit chamber wall, such a discrepancy is expected. It is noted that the maximum density (with respect to time) does drop very fast from the peak at the incident boundary to 20% of it after 1 inch of the propagation distance, which confirms the analysis we did in the previous section. In Fig. 6 (c), the transmitted pulse is shown as a function of time. It is clear that no abnormal "tail erosion" exists. The pulse is only distorted slightly in the tail part which suffers a small attenuation by the self-generated plasma.

Figs. 7 (a), (b) and (c) show the spectra of the incident and the transmitted pulse, the density profile as a function of time and space, and the transmitted pulse as a function of time respectively for $P=1.3P_c$. The frequency up-shift shown in Fig. 7 (a) is 0.39 MHz, which again agrees with the experiment. The maximum (with respect to time) density profile in Fig. 7 (b) again agrees with the measured one shown in Fig. 4 (a). The transmitted pulse shown in Fig. 7 (c) experiences more attenuation in the tail portion than that in Fig. 6 (c). It is expected since the plasma density is higher in this case than that of the previous case.

The agreements between the experimental measurements and the results of the numerical simulations on the amounts of frequency up-shift, the spectra of the transmitted pulses and the density distribution of the self-generated plasmas validate the theoretical model established in the first section of this chapter. One can use this model to guide the future experiments, predict the results of the planned experiments, and analyze the effect of various processes on the frequency conversion.

We have so far studied the frequency conversion phenomenon of a microwave pulse propagating in a self-generated plasma with low loss, and revealed only up-conversion phenomenon. How the frequency of a microwave pulse is shifted when the loss becomes significant is the subject discussed in the next section. The increase of tail

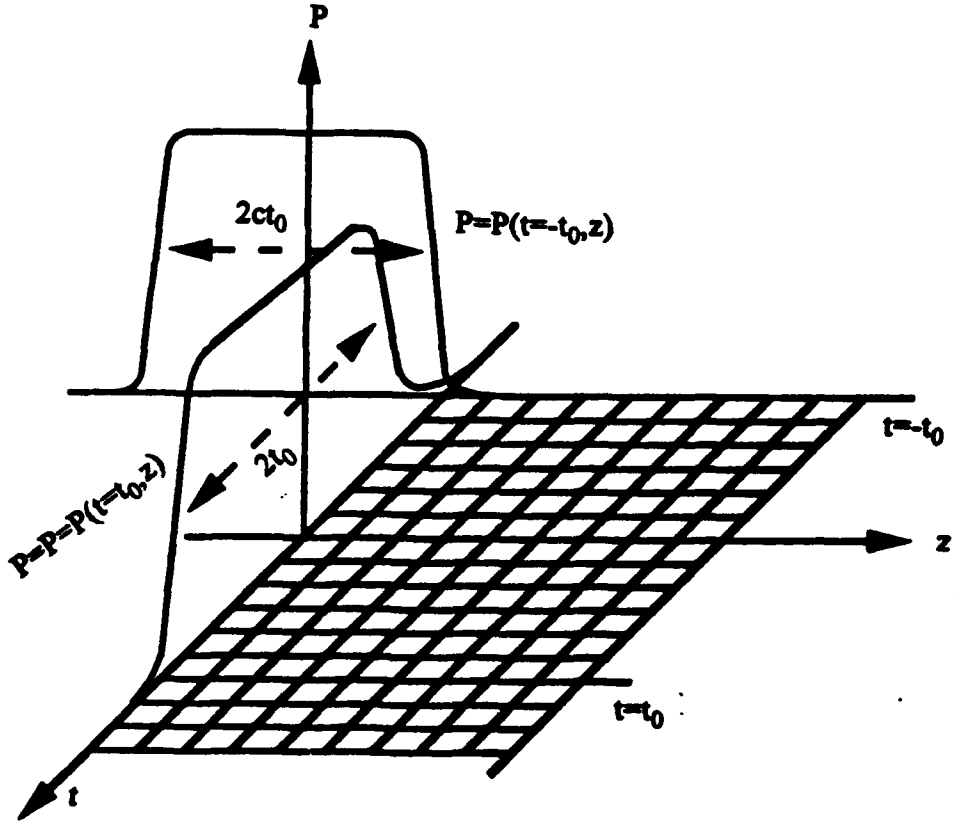

Fig. 5 Boundary and initial conditions for numerical simulations.

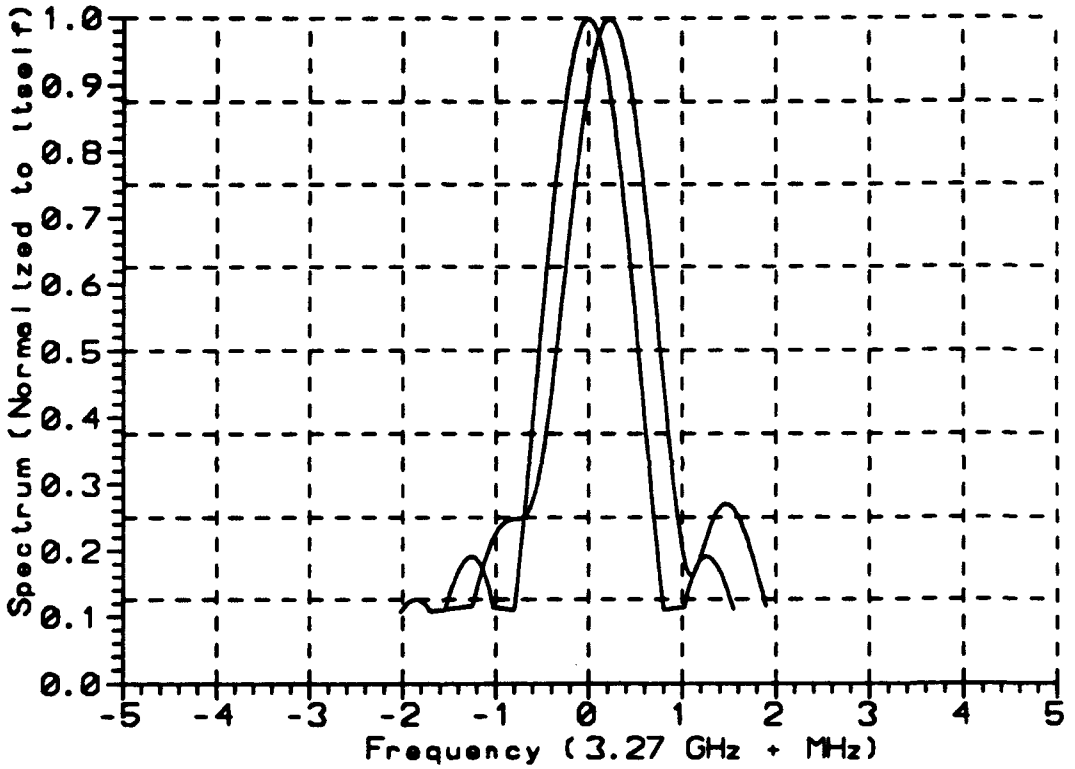

Fig. 6 (a) Numerical result of incident and transmitted pulse spectra for $P=1.1P_c$

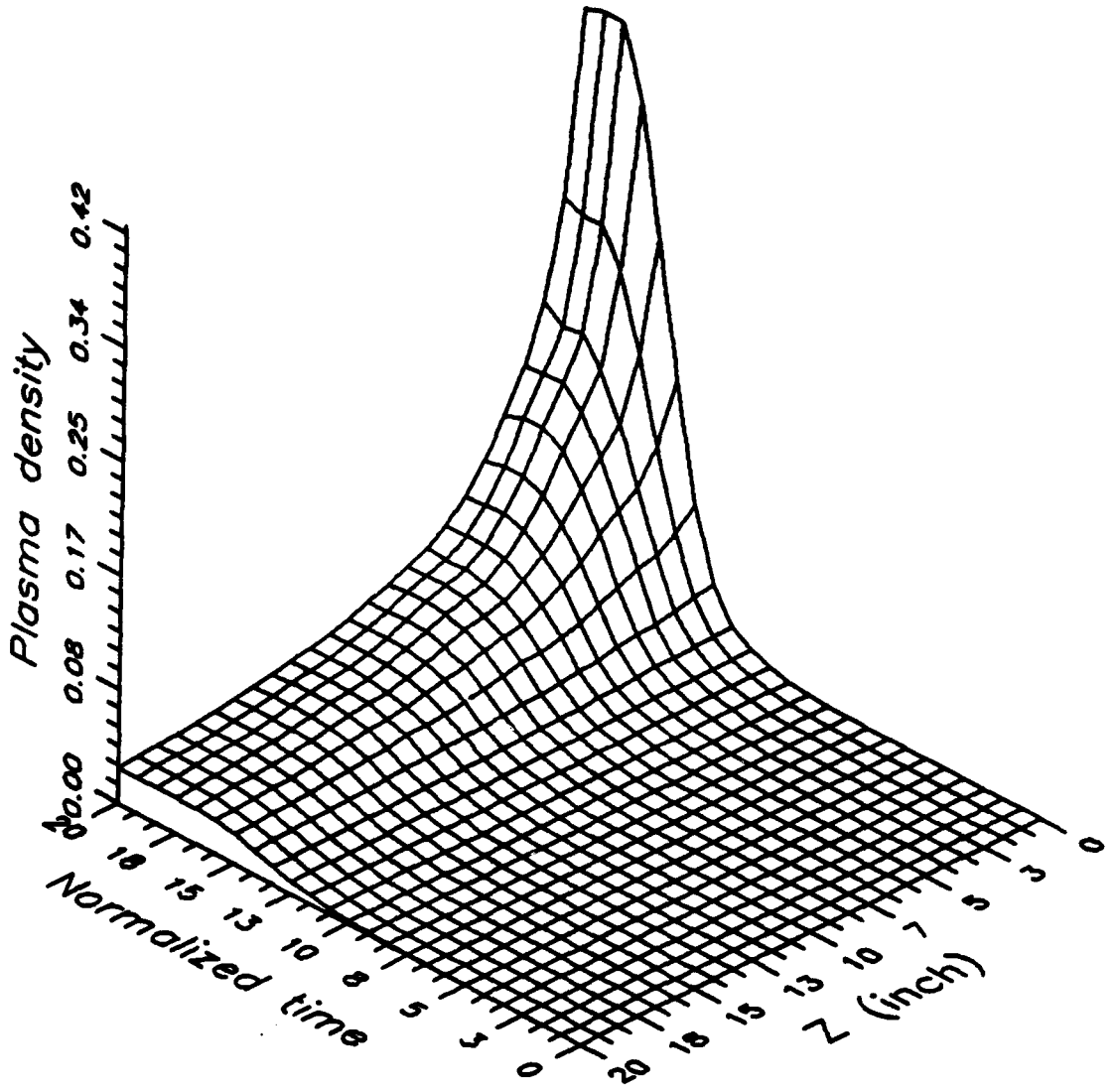

Fig. 6 (b) The numerical result of normalized plasma density vs. distance z and normalized time t. $P=1.1P_c$

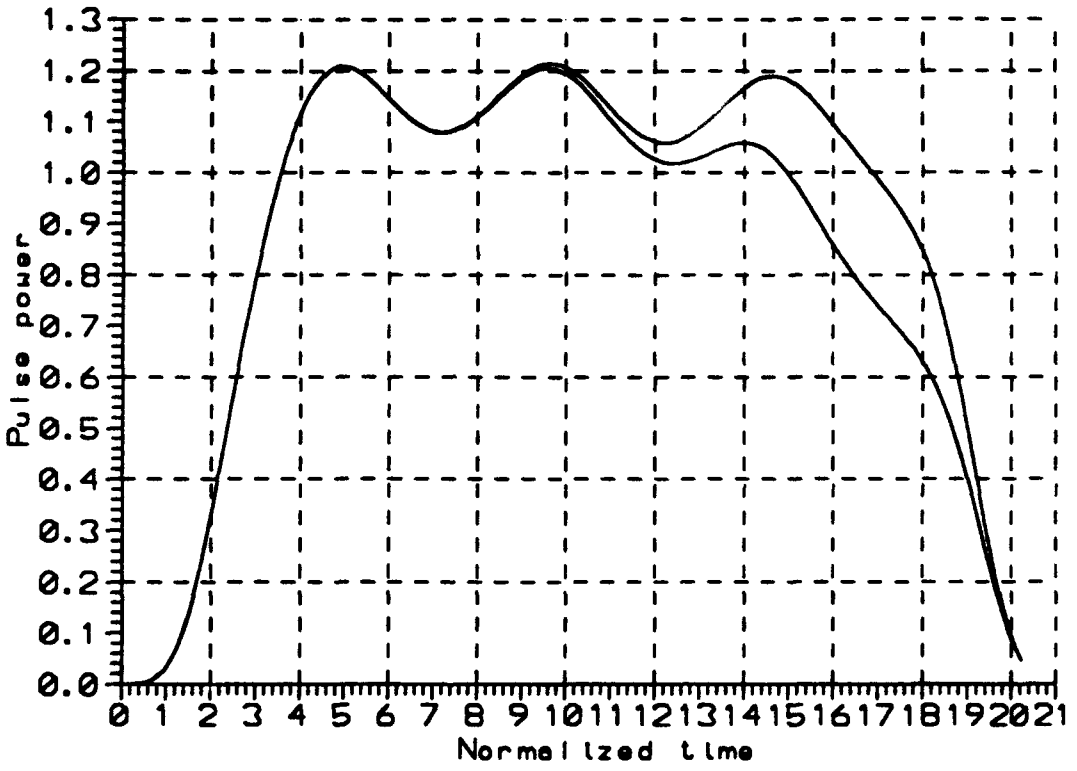

Fig. 6 (c) Numerical result of incident and transmitted pulse power for $P=1.1P_c$

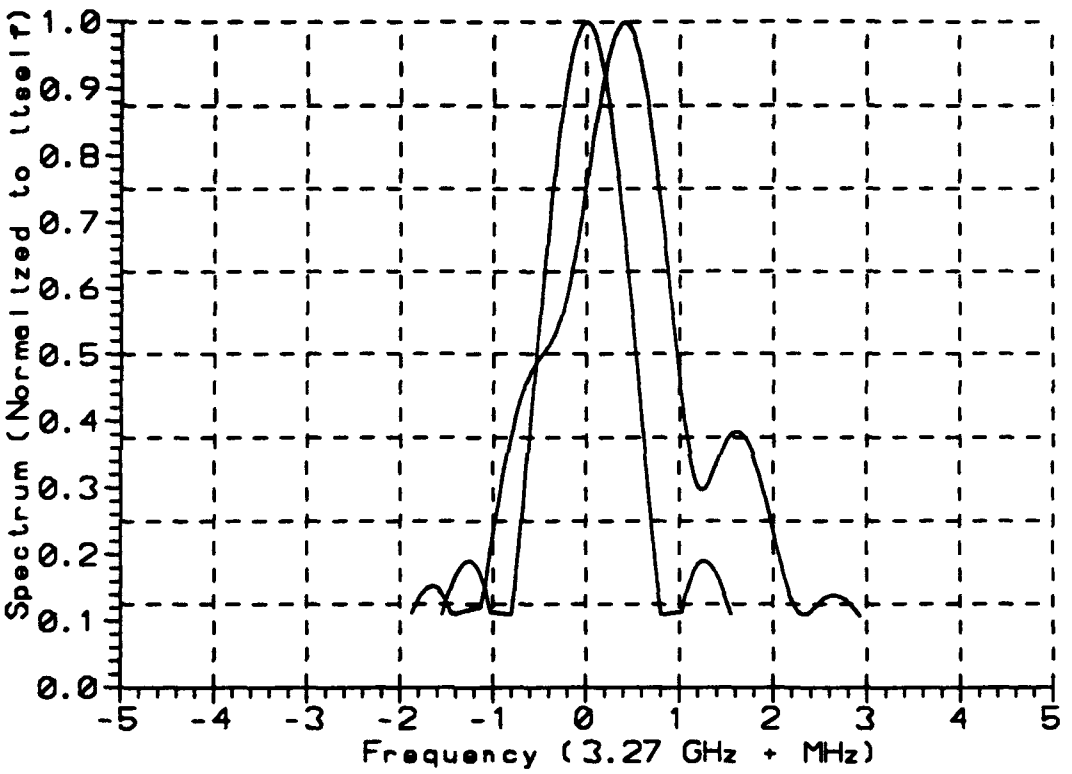

Fig. 7 (a) Numerical result of incident and transmitted pulse spectra for $P=1.3P_c$

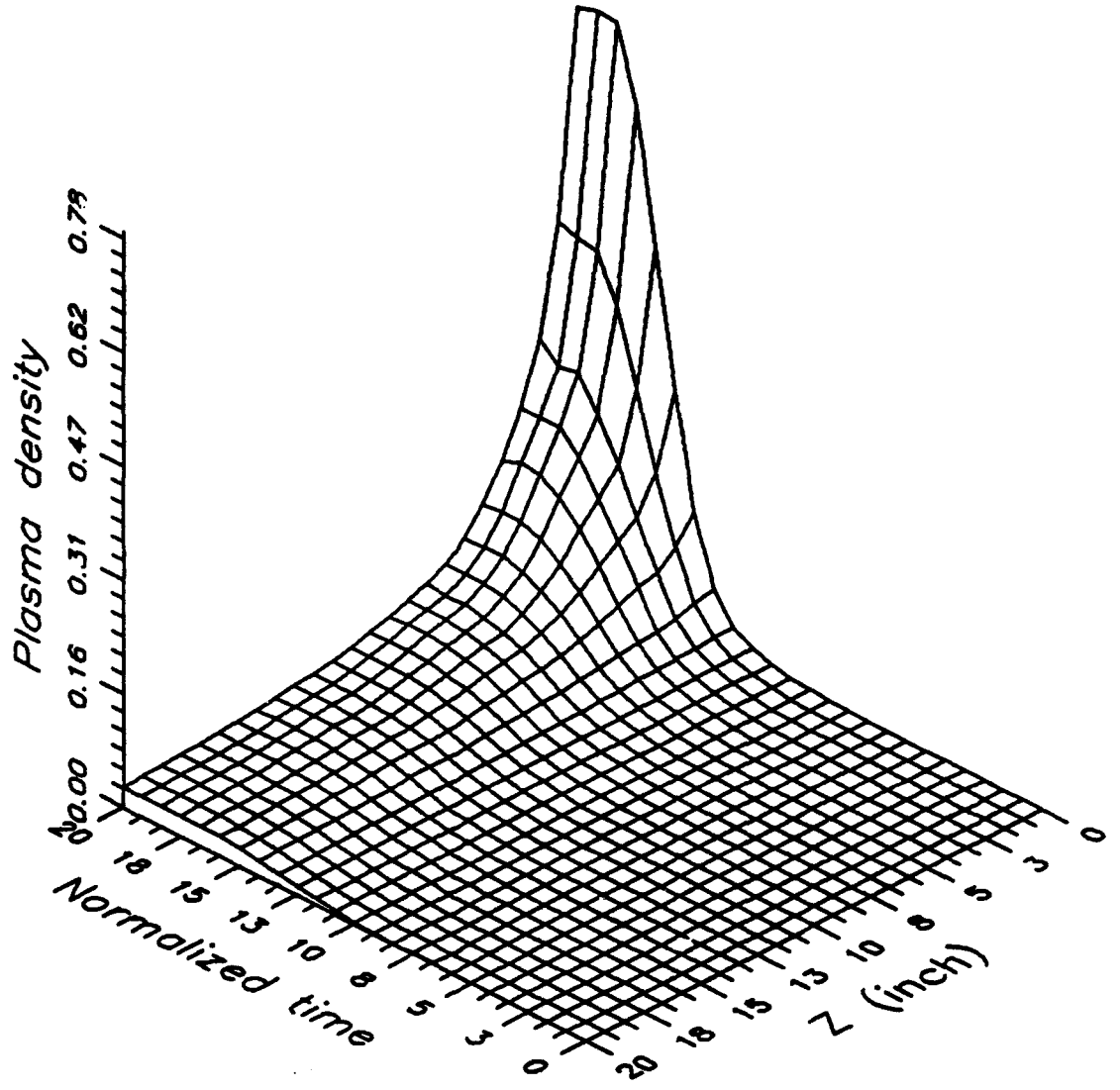

Fig. 7 (b) The numerical result of normalized plasma density vs. distance z and normalized time t. $P=1.3P_c$

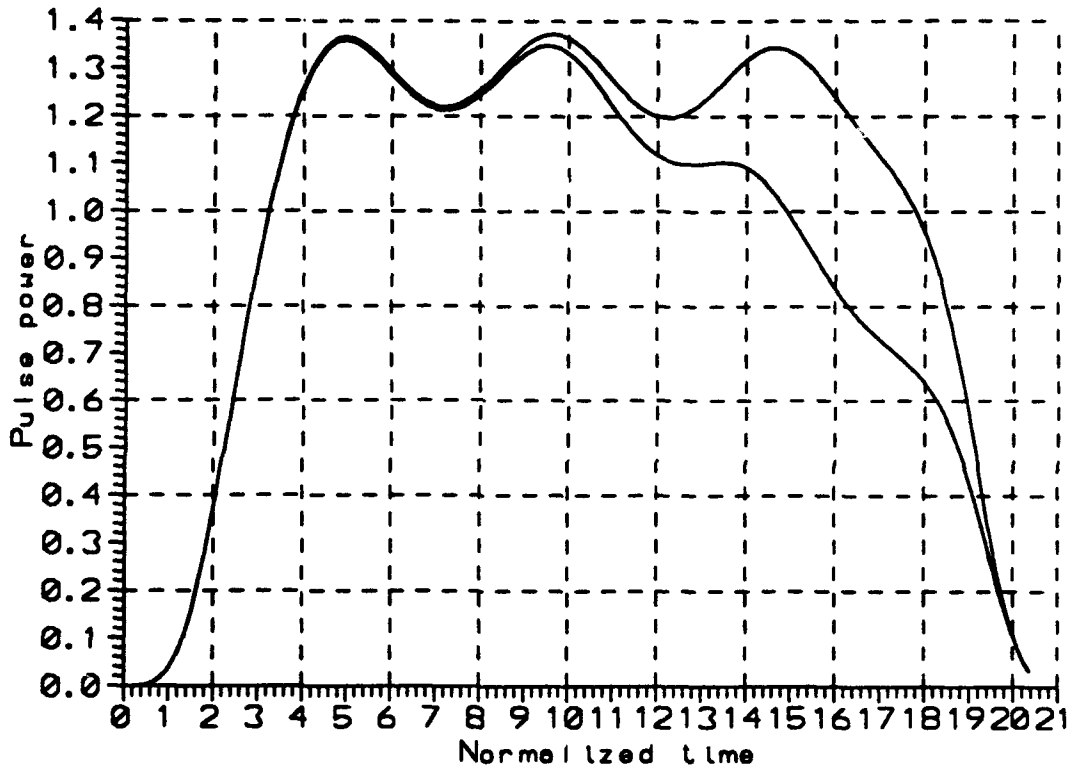

Fig. 7 (c) Numerical result of incident and transmitted pulse power for $P=1.3P_c$

erosion (i.e. loss) is done by increase the power of the incident pulse and raising the background pressure.

4. Experiments with consecutive increase of the microwave pulse power leading to spectral breaking phenomenon

In section 1, it was shown that if the loss of a plasma is too large the first term of equation (14) can not be neglected then (14) is rewritten as (15') and the condition on frequency up-shift of a rectangular pulse interacting with the self-generated plasma may not hold. In other words, the time varying plasma may also cause frequency down-shift. It has been observed in many experiments[1,2] that frequency down-shifted spectral lines have also appeared in the recorded spectra. The reason of relating the result of frequency down-shift to the loss of the pulse in the plasma is based on the dispersion relation $\omega^2 = \omega_{pe}{}^2 + k^2c^2 - \nu^2$ of a wave in a collisional plasma, which indicates that collision (i.e. loss) tends to lower the resonance frequency of the plasma. When plasma is created by the wave, the ionization loss of the wave gives rise to an effective collision frequency which modifies the collisionless dispersion relation of the wave to the form of collisional case. Thus, a frequency down-shift to the wave may result. However, this physical interpretation is not as obvious as that for frequency up-shift case. Therefore, the identification of the role of electron effective collision frequency in causing frequency down-shift needs an effort of a systematic study, including theoretical formulation, experimental demonstration, and computer simulation and experiments.

Using the same experimental set up as in Fig. 2 (b), the experiments are performed with consecutive increase of the incident power exceeding the levels of the experiments presented in section 2. More dense plasma will be generated by the higher power, thus,

the effect of loss becomes more significant for the purpose of study. The air pressure in the chamber is set to be about 0.2 torr. At this pressure, the breakdown threshold is lower than the previous experiments in which the pressure was 0.08 torr and beyond the Paschen minimum. The electron-neutral collision frequency is about $1.2\times10^9\sqrt{T_e}\ s^{-1}$, where T_e is the electron temperature measured in eV as in section 2. In order to avoid the undesired boundary effect, i.e., over ionization to cause cutoff reflection of the incident pulse at the incident boundary, the intensity of the incident pulse is limited to no more than 50% above the breakdown threshold power level. Consequently, the ionization frequency of the background gas is of the same order of magnitude as the electron-neutral collision frequency in the present experiments. Thus the amount of frequency up-shift and down-shift will be of the same order of magnitude and the cause of frequency down-shift can be examined conveniently.

The results of the experiments performed with a sequence of pulses having consecutively increasing incident powers are presented in the following. Shown in Figs. 8 (a)-(f) are the recorded spectra of the incident and transmitted pulse for $P=1.05P_c$, $P=1.08P_c$, $P=1.14P_c$, $P=1.17P_c$, $P=1.32P_c$, and $P=1.37P_c$, respectively. The peaks of the transmitted pulses in Figs. 8 (a), (b) and (c) are shown to be up-shifted from the carrier frequency 3.27 GHz of the incident pulses. The up-shifted quantities are 0.08 MHz, 0.26 MHz and 0.45 MHz, respectively. Moreover Fig. 8 (c) shows that the spectrum of the transmitted pulse starts to become non-symmetrical and spectrum in Fig. 8 (d) start to break up, a down-shift component emerges. Figs. 8 (e) and (f) show an even more pronounced result. The spectra of the transmitted pulses have two clear peaks. One is up-shifted and the other one down-shifted from the single peak location of the incident pulse. The amount of frequency down-shift is also comparable to that of the up-shifted frequency in both cases.

The theoretical model presented in Section 1 can be used here to numerically simulate the experiments as well. Using the experimental parameters, i.e., let the pressure

be 0.2 torr and the collision frequency $\nu=10\nu_0(P+0.03)^{1/2}$, where $\nu_0=3.99\times10^9 p/\omega_0$, the spectra of the transmitted pulses for incident pulses having $P=1.05P_c$, $P=1.08P_c$, $P=1.14P_c$, $P=1.17P_c$, $P=1.32P_c$, and $P=1.37P_c$ are calculated. Figs. 9 (a)-(f) show the results of the numerical simulations. Comparing the spectra in Figs. 9 (a)-(c) to those in Figs. 8 (a)-(c), good agreements are shown. The amount of frequency up-shift deduced from Figs. 9 (a)-(c) are 0.08 MHz, 0.23 MHz and 0.45 MHz, respectively, which are also excellently matched with the experimental results. The spectral breaking phenomenon shown in Figs. 8 (d)-(f) also appears in the results of the numerical simulation as shown in Figs. 9 (d)-(f). This consistency further validates the theoretical model presented in Section 1. To identify the role of effective collision frequency plays in causing the frequency down-shift and spectral breaking, a series computer experiments are performed based on the validated theoretical model and presented in next section.

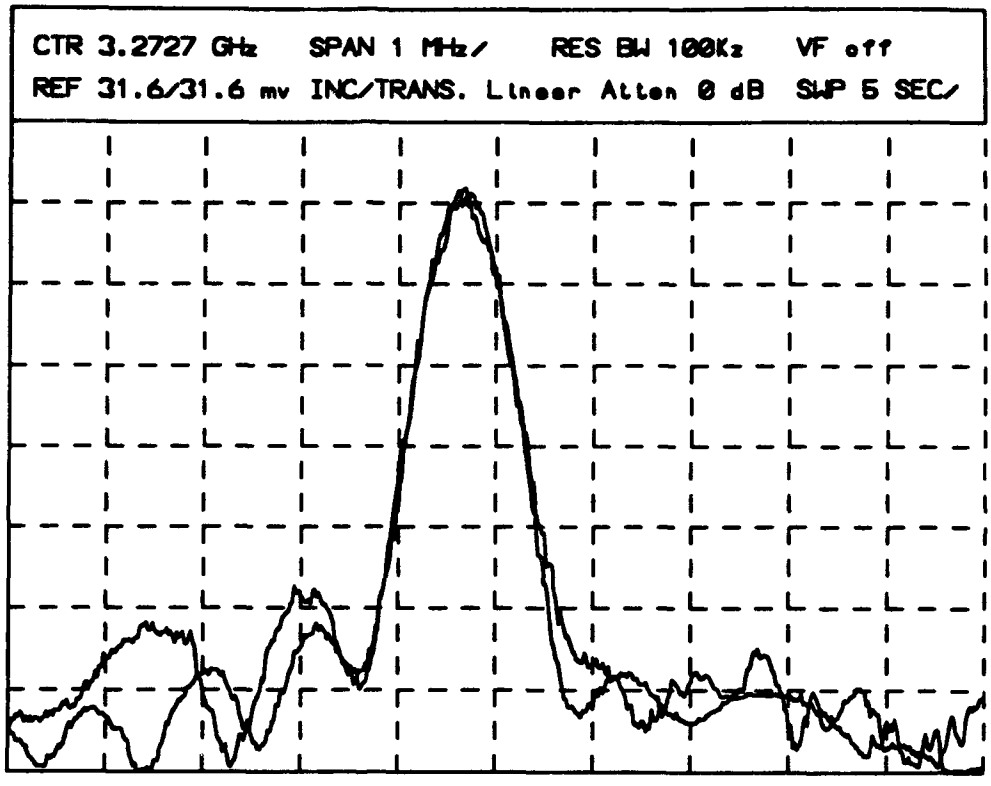

Fig. 9 (a) The recorded spectra of the incident and transmitted pulse with incident pulse power for $P=1.05P_c$

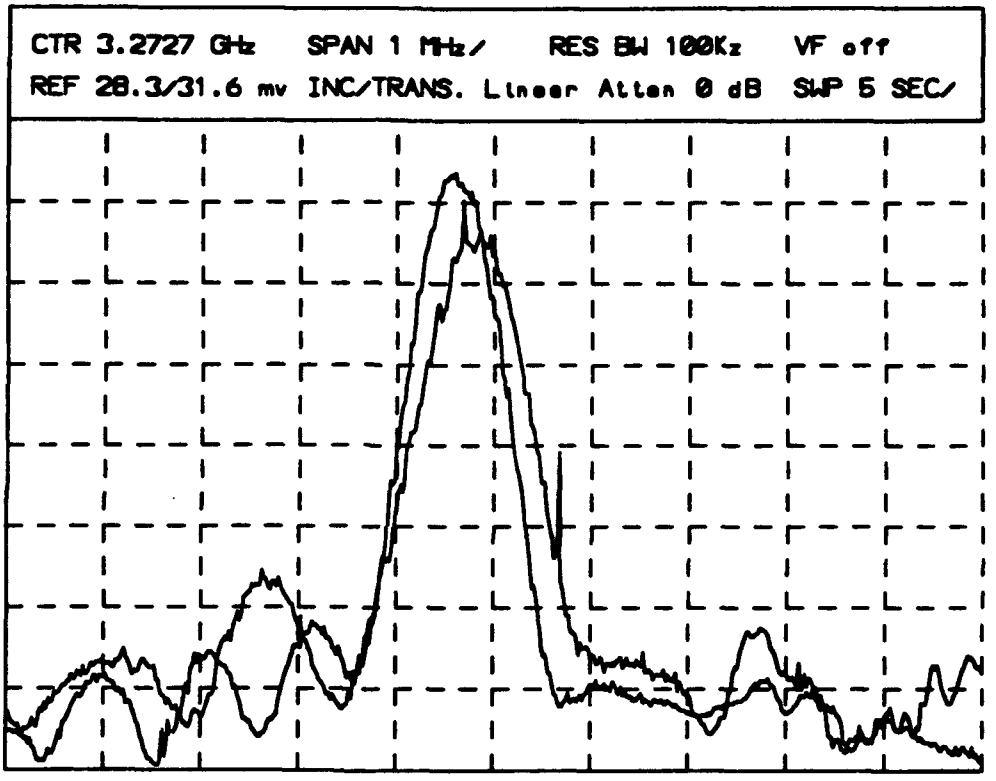

Fig. 8 (b) The recorded spectra of the incident and transmitted pulse with incident pulse power for $P=1.08P_c$

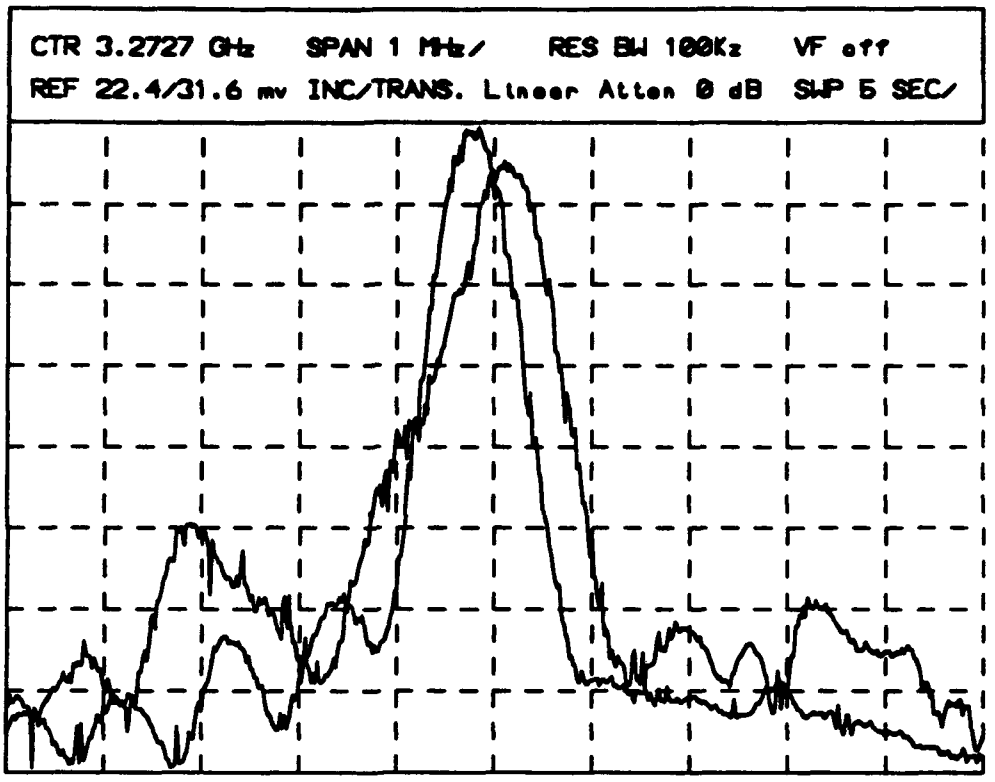

Fig. 8 (c) The recorded spectra of the incident and transmitted pulse with incident pulse power for $P=1.14P_c$

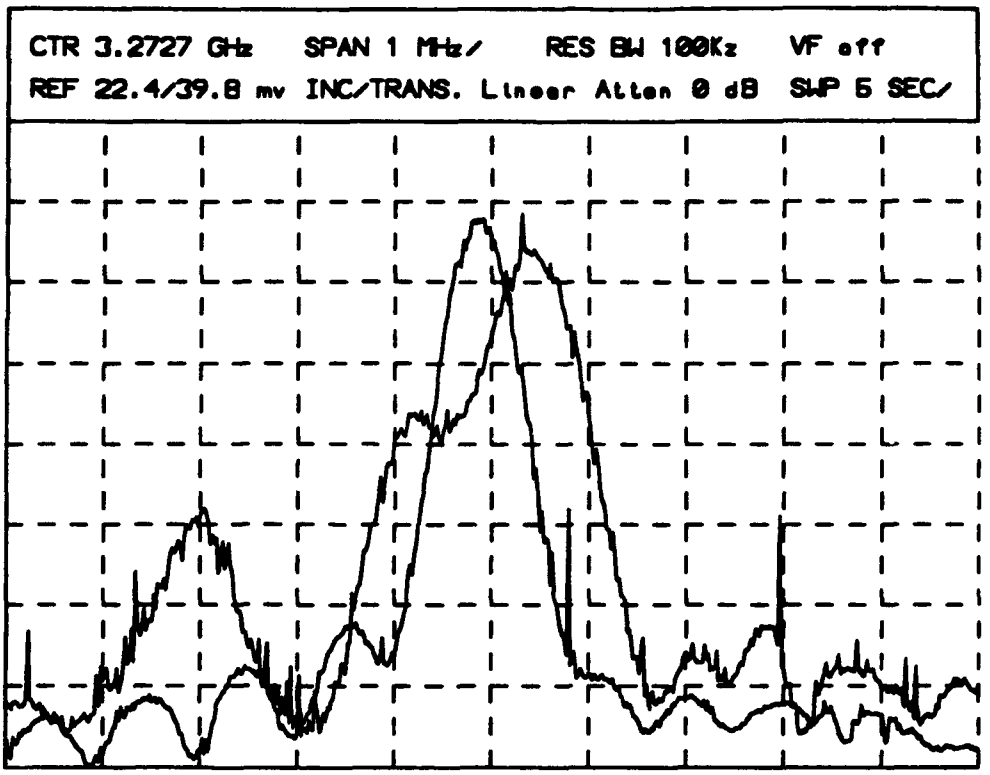

Fig. 8 (d) The recorded spectra of the incident and transmitted pulse with incident pulse power for $P=1.17P_c$

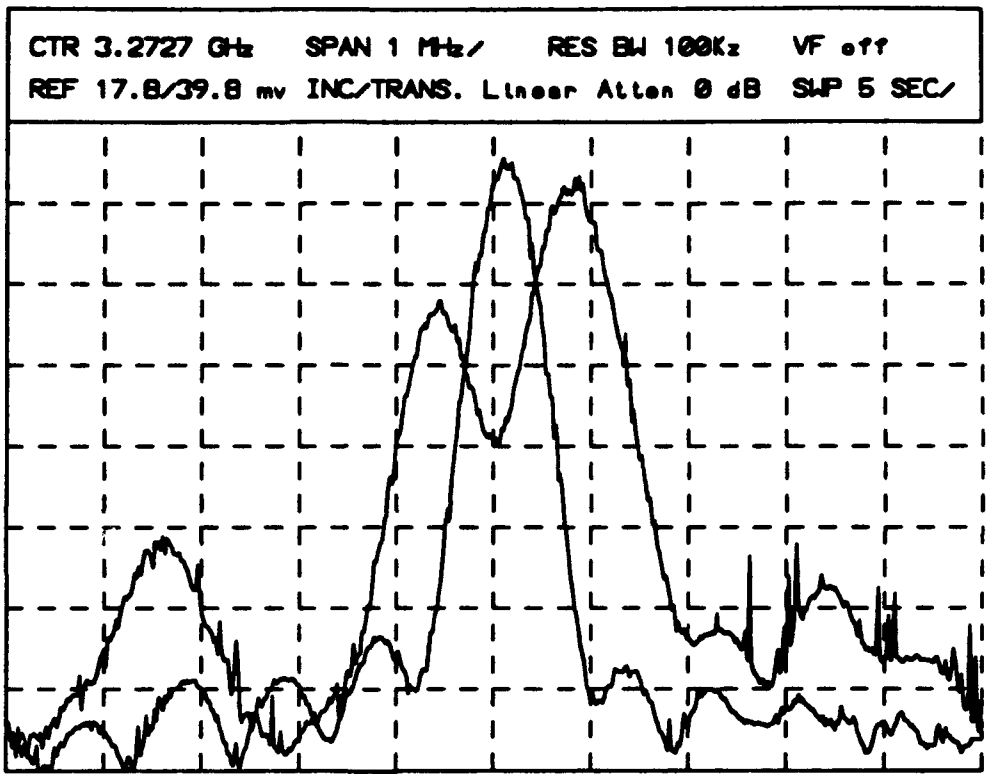

Fig. 8 (e) The recorded spectra of the incident and transmitted pulse with incident pulse power for $P=1.32P_c$

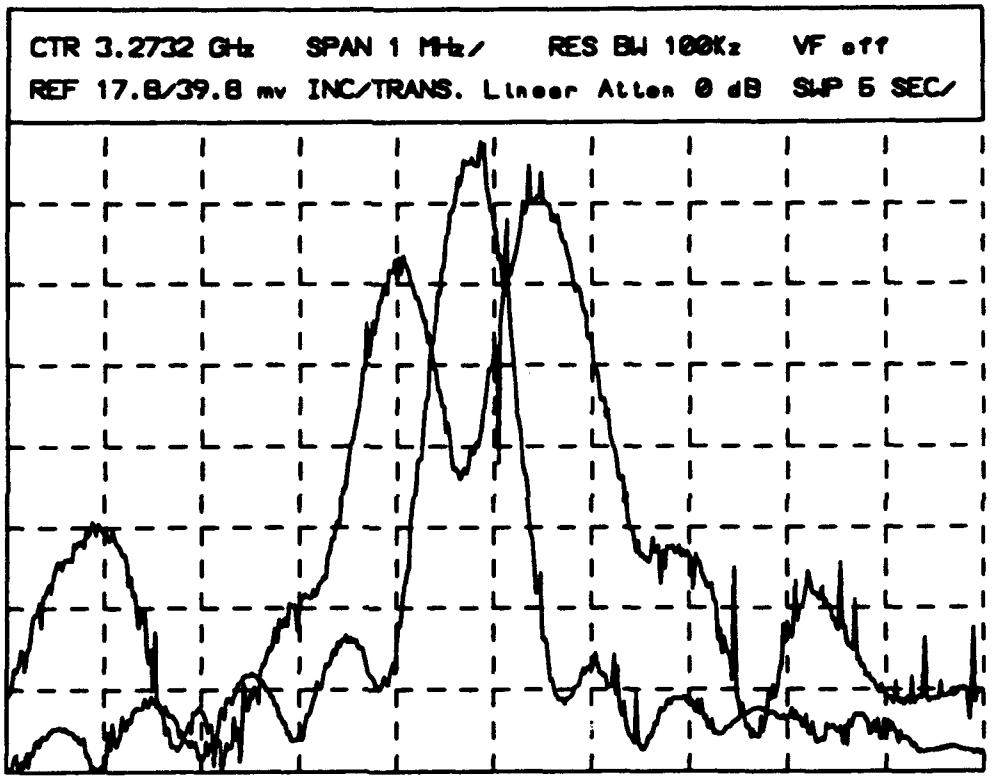

Fig. 8 (f) The recorded spectra of the incident and transmitted pulse with incident pulse power for $P=1.37P_c$

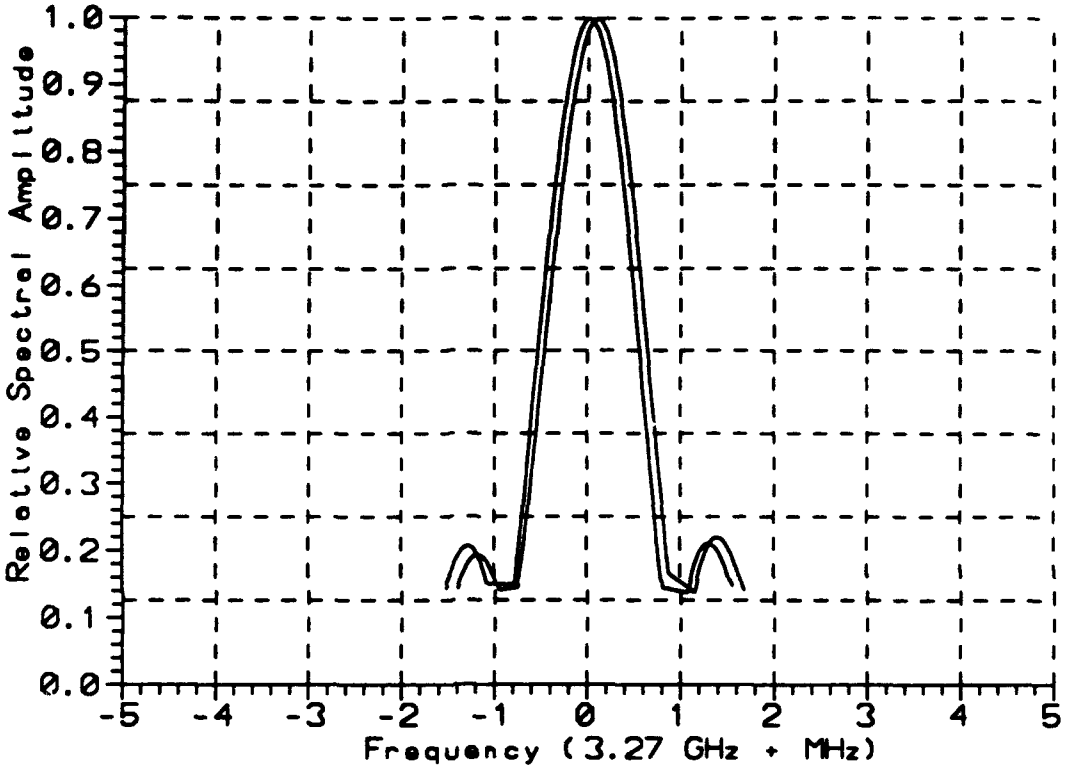

Fig. 9 (a) The numerical result of the spectra of the incident and transmitted pulse for $P=1.05P_c$

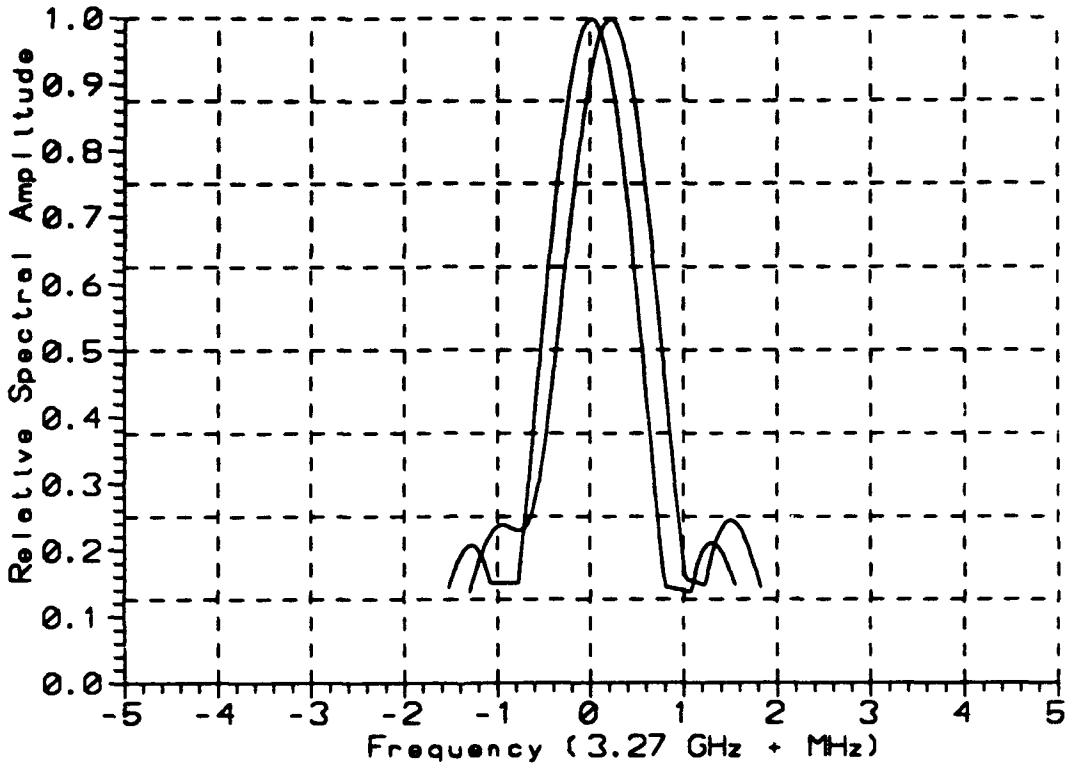

Fig. 9 (b) The numerical result of the spectra of the incident and transmitted pulse for $P=1.08P_c$

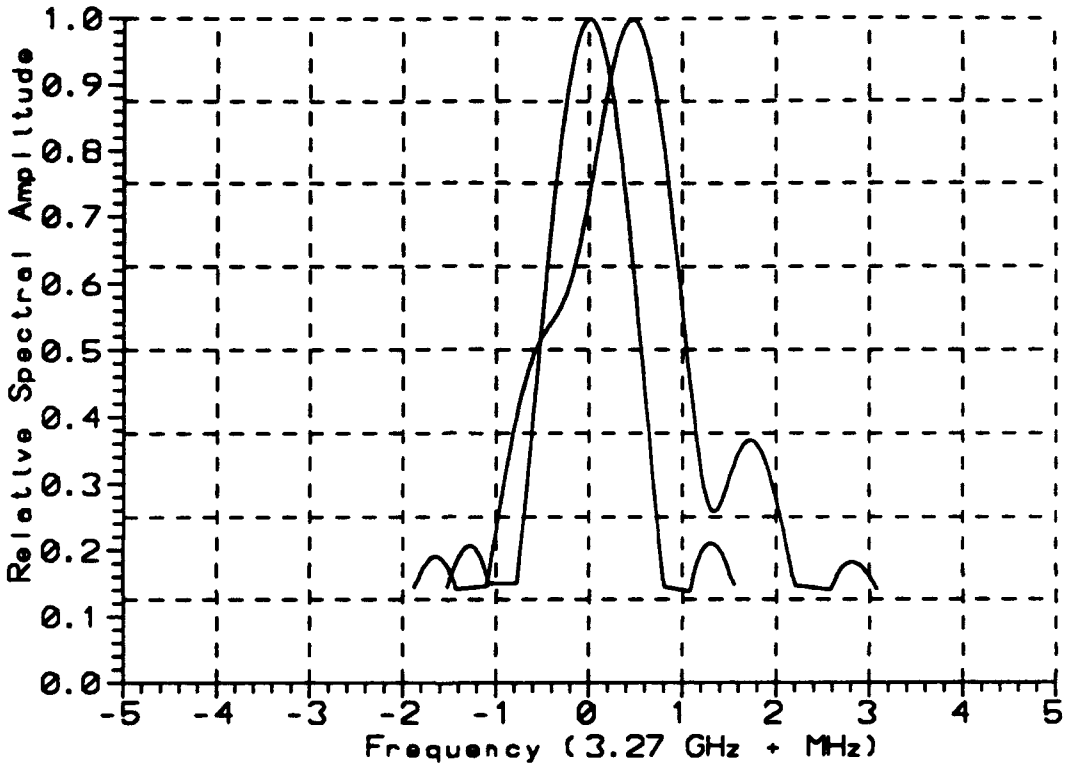

Fig. 9 (c) The numerical result of the spectra of the incident and transmitted pulse for $P=1.14P_c$

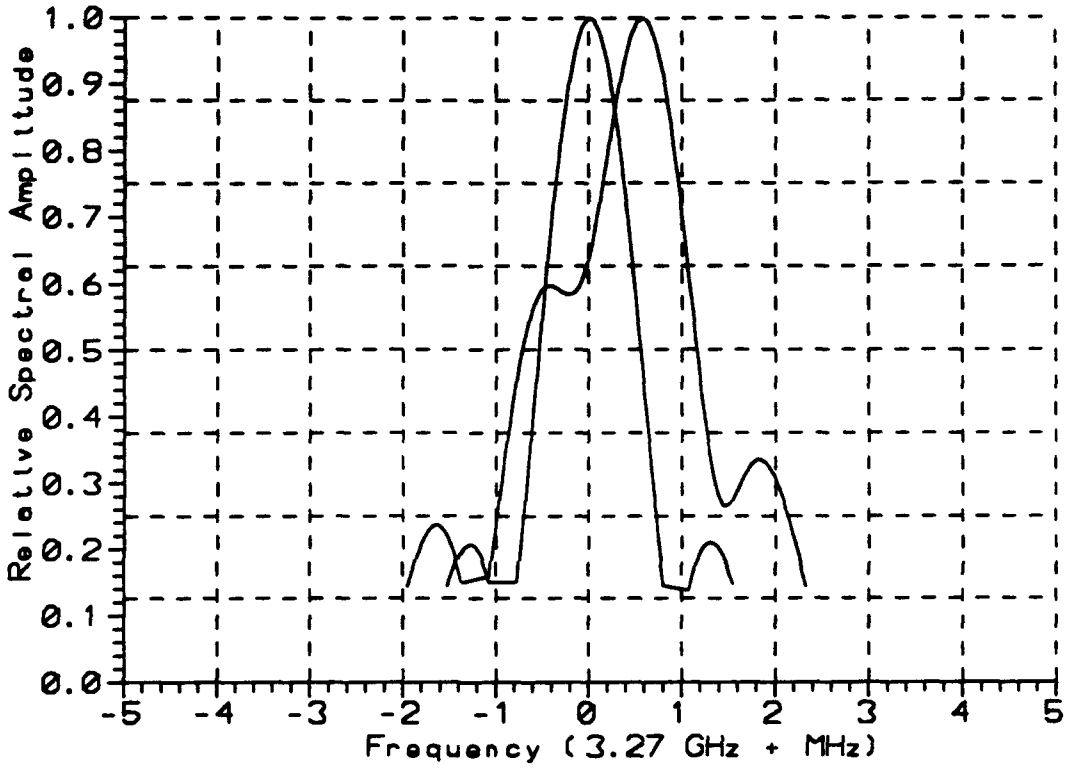

Fig. 9 (d) The numerical result of the spectra of the incident and transmitted pulse for $P=1.17P_c$

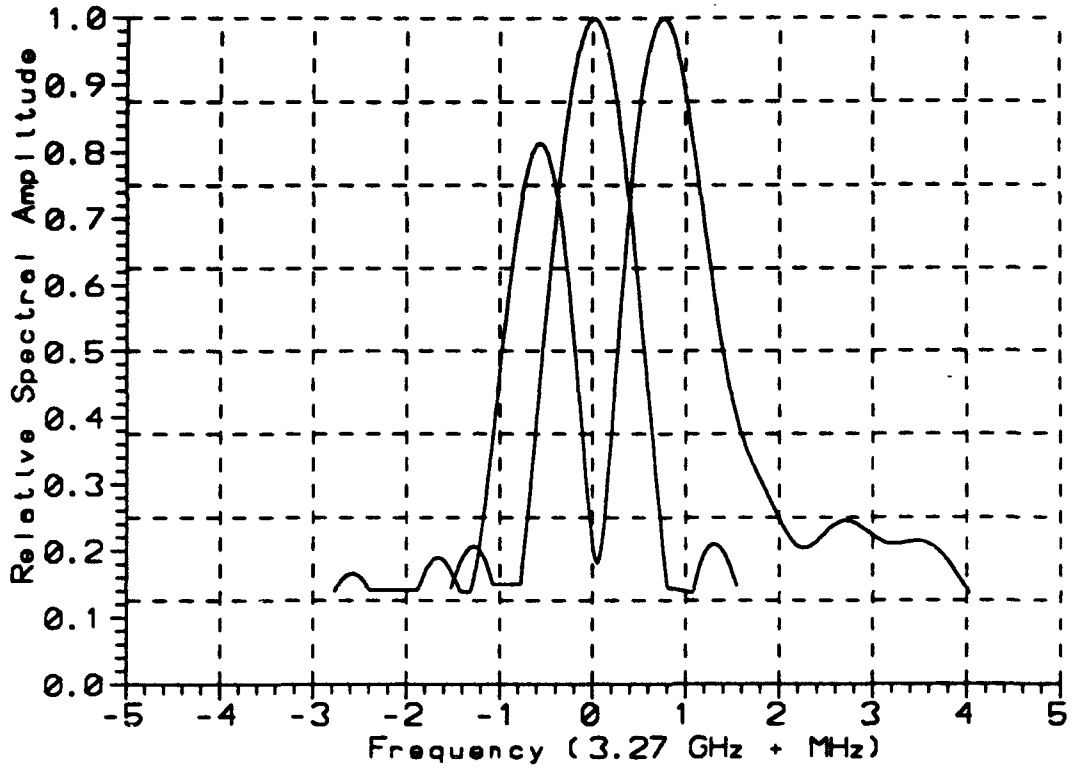

Fig. 9 (e) The numerical result of the spectra of the incident and transmitted pulse for $P=1.32P_c$

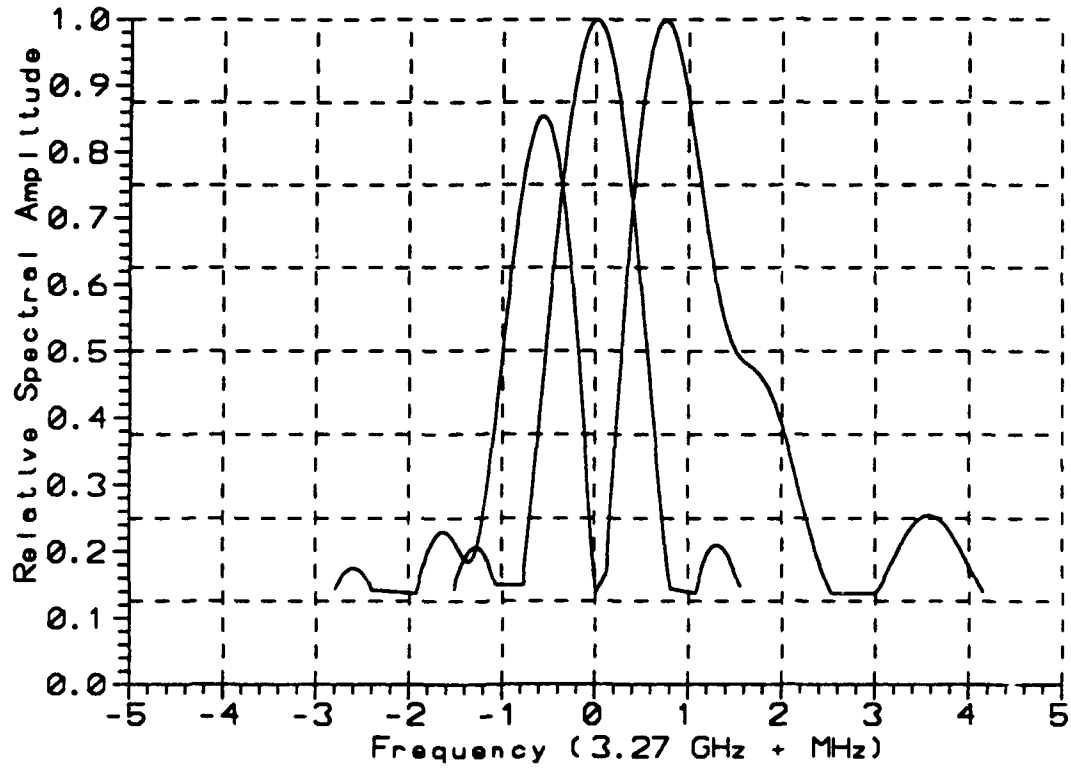

Fig. 9 (f) The numerical result of the spectra of the incident and transmitted pulse for $P=1.37P_c$

5. Computer experiments to identify the collision loss as the mechanism causing frequency down-shift and spectral breaking

To verify that the collisional loss indeed contributes to the mechanism causing frequency down-shift, a series of computer experiment are conducted. It is done by multiplying a variable parameter ξ to the electron-neutral collision frequency ν in equations (17), (18) and (19) and varying ξ from 0.5 to 2. In general, ν_i and ν_a are proportional to ν, however, their relationships are removed artificially in the computer experiment. In other words, only the electron-neutral collision frequency ν is varied artificially for a fixed background condition. In doing so, the role of ν on frequency down-shift may be identified unambiguously.

Presented in Fig. 10 is the dependencies of the amounts of frequency down-shift $-\Delta f_d$ on ξ for different incident power levels. A monotonic increase of $-\Delta f_d$ with ξ is observed for all different incident powers. $-\Delta f_d$ also varies with the power of the incident pulse, P. It increases with P, and then reaches a saturation level as manifested by the overlap of the curves. On the other hand, the dependencies of the amounts of frequency up-shift Δf_u on ξ and P presented in Fig. 11 show that Δf_u decreases monotonically with ξ, but increases with P, then reaches a saturation level. The frequency f_m , the minimum between the up-shift peak and down-shift peak of the spectrum of the transmitted pulse, also varies with ξ and P. The dependencies of $\Delta f_m (=f_m - f_0)$ on ξ and P are presented in Fig. 12. Similar to Δf_u , Δf_m decreases with ξ and increases with P, then reaches a saturation level, as shown in Fig. 12. These results clearly demonstrate that ξ plays an important role in determine frequency shift, in particular, in introducing the down-shifted frequency components in the spectrum of the transmitted pulse.

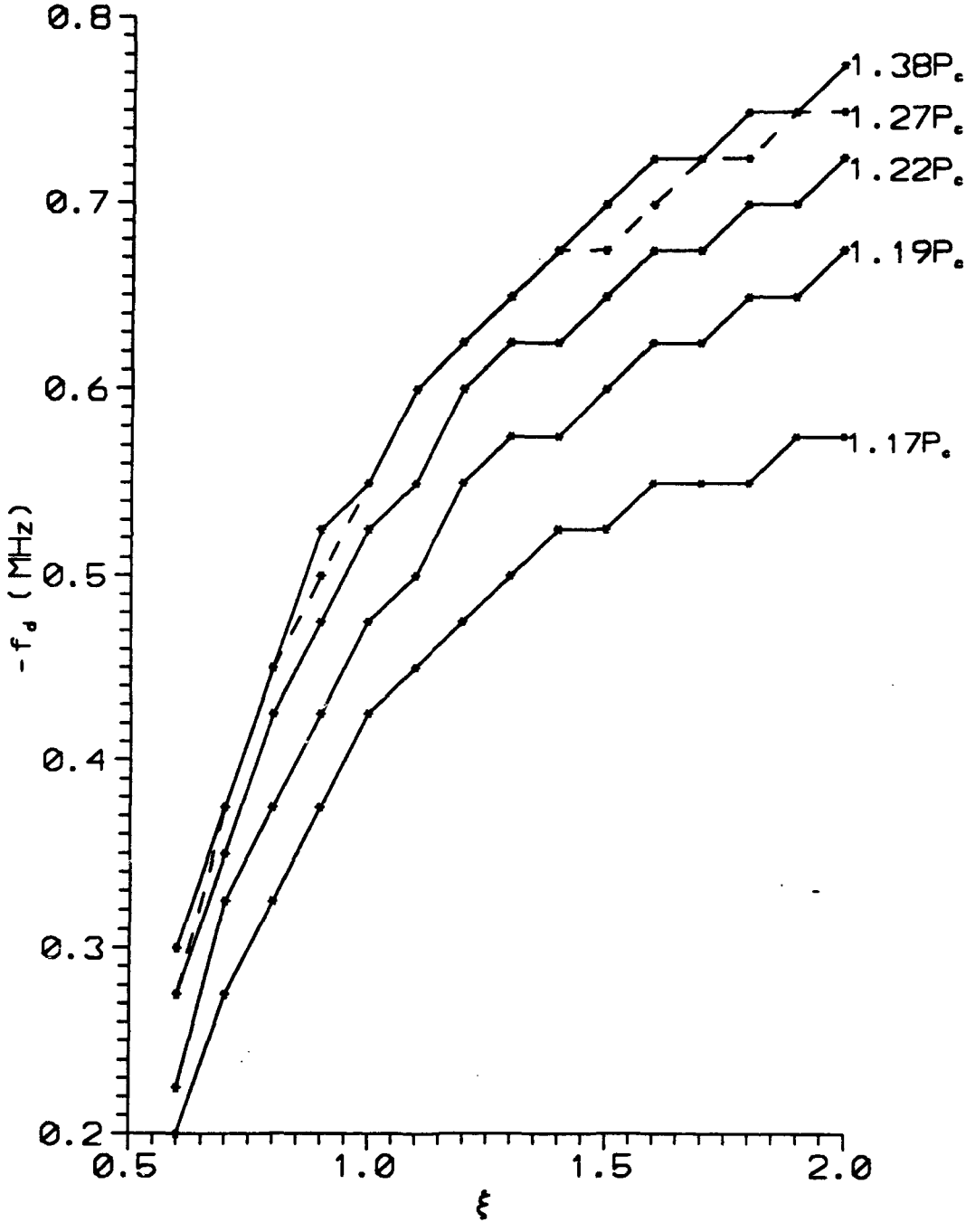

Fig. 10 $-\Delta f_d$ vs ξ and P

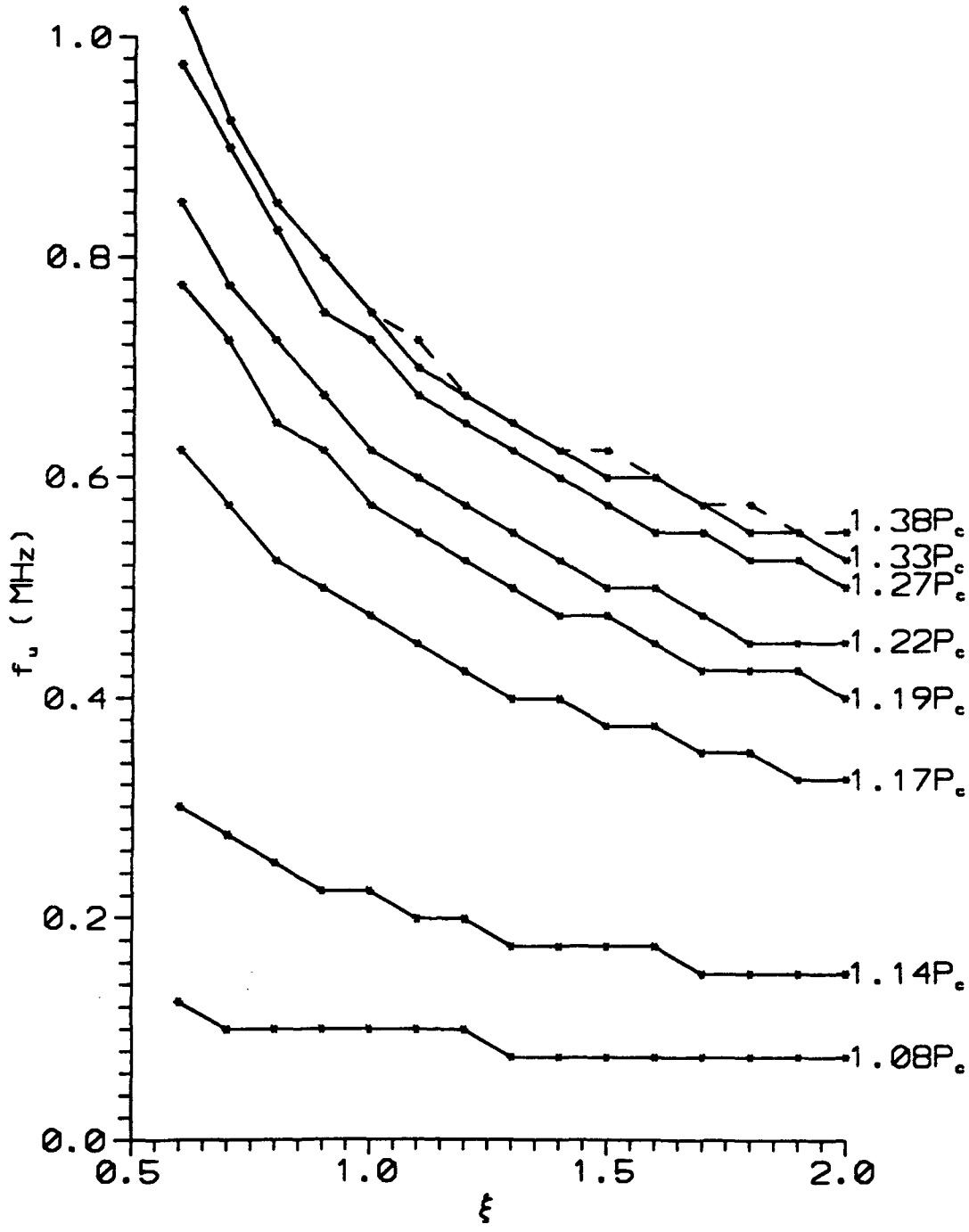

Fig. 11 Δf_u vs ξ and P

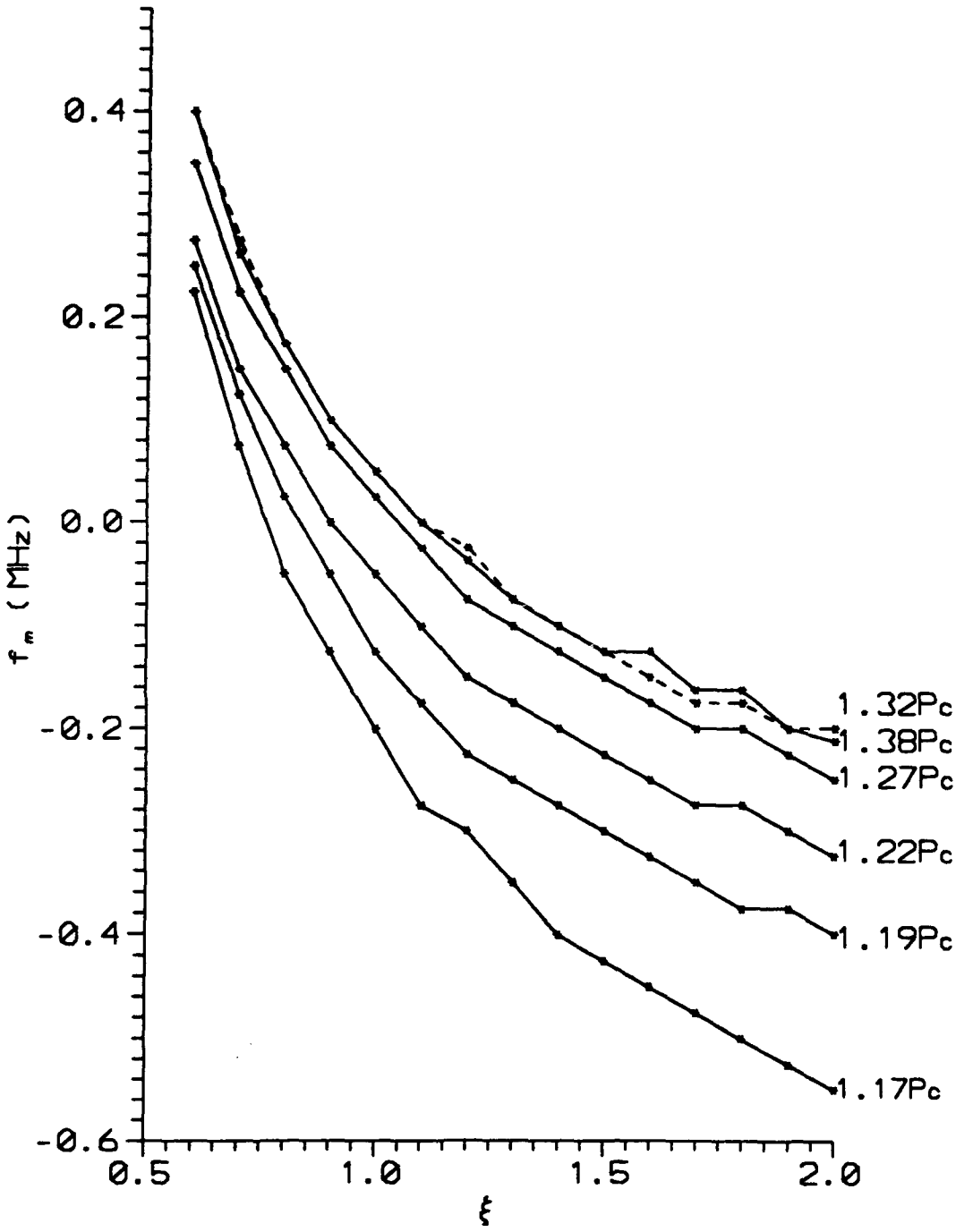

Fig. 12 Δf_m vs ξ and P

6. Summary

The study of frequency conversion of a high power microwave pulse propagating in a self-generated plasma is presented in this chapter. The theoretical model is first presented and the equation describing the frequency auto-conversion process is derived. It indicates that under the condition of $\nu_1\nu_2 << (\omega^2+\nu_2^2)$ the carrier frequency of the microwave pulse will be up-shifted. If the carrier frequency is greater than the plasma frequency at the incident boundary, during the propagation the carrier frequency of the pulse will be up-shifted continuously to be always higher than the plasma frequency of the self-generated plasma. Thus, there is no cutoff reflection and the erosion of the pulse energy by the self-generated plasma is minimized. Both the chamber experiments and the numerical simulations confirm this theoretical prediction of frequency up-shift phenomenon. For quantitative comparison, a photomultiplier, which has been calibrated by the results of a double Langmuir probe, is used to measure the electron density distribution along the path of the pulse. This measured distribution agrees with the distribution obtained by numerical simulation. Using the measured electron density distribution, the predicted amount of frequency up-shift can be evaluated by the formula derived from the theoretical model. Again a good agreement is obtained among the theoretical prediction (with the aid of experimentally measured electron distribution), experimental observation, and computer simulation.

In the situation that the loss of the pulse in the self-generated plasma becomes significant, i.e. the effective collision frequency $(\nu_1\nu_2)^{1/2}$ is high comparing with the plasma frequency, frequency down-shift components appear together with the frequency up-shift components in the spectrum of the transmitted pulse. In other words, the spectrum of the pulse breaks up into two peaks up and down-shifted from the original carrier frequency. The results of the computer experiments based on the theoretical model show that the collision frequency and the incident power are the two factors causing the frequency down-shift and spectral breaking. Since the loss of the pulse increases with the

incident power, the two factors are combined into one effective collision frequency. Therefore, it is the effective collision frequency which plays a major role in the process of frequency down-shift and spectral breaking. Physically, it is realized by the fact that electron collisions reduce the phase velocity of the wave in the plasma as indicated by the dispersion relation. The increasing dependence of frequency down-shift on electron-neutral collision frequency observed in the computer experiments suggests that the frequency down-shift phenomenon recorded in the experiments is indeed caused by the effective collisionality of the plasma.

Chapter III

Frequency Up-shift of a Wave propagation through a Rapidly Created Plasma

The frequency up-shift of a cw wave propagating through a rapidly created plasma is the subject of this chapter. The plasma is produced by separate means (instead of the propagating wave itself). Hence, in this chapter, the plasma density is not related to the wave intensity as the case discussed in chapter II.

1. The theoretical model for cw wave propagating in a rapidly created plasma.

The problem considered here involves a cw wave propagating through a fast growing plasma slab which is located between z=0 and L. A schematic of the problem is illustrated in Fig. 13. The variation of the plasma density in the slab is modeled as

$$\begin{aligned} n_e(z,t)&=u(t)g(z)n_{e0}\exp[\alpha_1(t)t] \ , \quad && 0<t<t_0, \text{ while plasma density is rising} \\ n_e(z,t)&=u(t)g(z)n_{e,max}\exp[-\alpha_2(t)t] \ , \quad && t>t_0, \text{ while plasma density is decaying} \end{aligned} \tag{24}$$

where u(t) is a unit step function, g(z)=1 for 0<z<L and 0 for z elsewhere, n_{e0} is the initial background plasma density, α_1 is the plasma rising rate depending on the ionization processes, $n_{e,max}$ is the maximum plasma density of the gas, $(0,t_0)$ is the ionization time interval, and α_2 is the plasma decaying rate depending on the loss processes. The relevant equation to wave propagation is the electron momentum equation

$$\frac{\partial}{\partial t}(n_e\bar{v}_e)=-n_e e\bar{E}/m_e \tag{25}$$

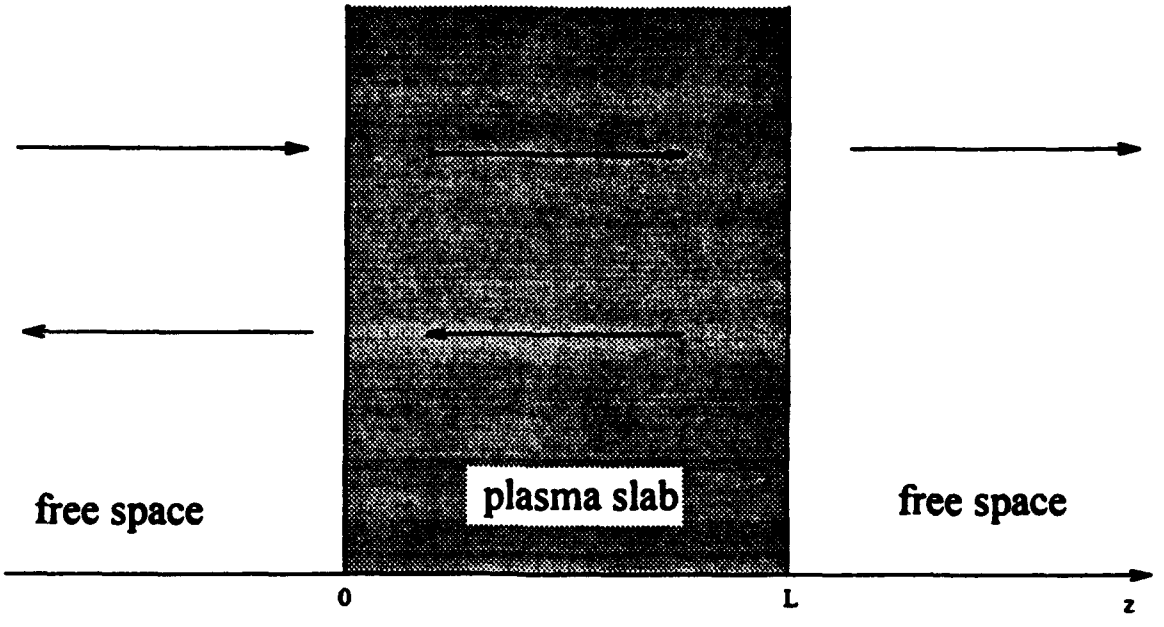

Fig. 13 cw wave propagating through a fast growing plasma slab, an initial and boundary value problem.

where $\vec{E}$ is the wave field; $\vec{v}_e$ is the electron velocity; and e and m_e are the electron charge and electron mass respectively. Combining equation (25) and the wave equation $\frac{\partial^2}{\partial t^2}\vec{E}-c^2\frac{\partial^2}{\partial z^2}\vec{E}=-4\pi\frac{\partial}{\partial t}\vec{J}$, one gets:

$$\frac{\partial^2}{\partial t^2}E-c^2\frac{\partial^2}{\partial z^2}E+\omega_{pe}^2E=0 \tag{26}$$

where $\omega_{pe}^2=4\pi n_e e^2/m_e$. Equation (26) together with equation (24) and boundary and initial conditions completely defines the wave propagating through a rapidly created plasma slab.

Since the electric field and magnetic field of the wave have to be continuous on the boundaries of the plasma slab, The boundary conditions are:

$$E(z=0^-,t)=E(z=0^+,t) \text{ and } E(z=L^-,t)=E(z=L^+,t) \tag{27}$$

and

$$\frac{\partial}{\partial z}E(z=0^-,t)=\frac{\partial}{\partial z}E(z=0^+,t) \text{ and } \frac{\partial}{\partial z}E(z=L^-,t)=\frac{\partial}{\partial z}E(z=L^+,t) \tag{28}$$

Outside the plasma slab, wave propagates in free space and the radiation condition can be used to derive the additional conditions for solving the wave equation (26). On the incident side (left-hand side in Fig. 13) of the plasma slab, there is a cw wave propagating toward the right (z direction) and a reflected wave from the incident boundary of the plasma slab, hence, the total wave field in the region is:

$E(z=z_1,t)=E_0\cos(\omega_0 t-k_0 z_1)+E(z=z_1+\Delta z,t-\Delta t)-E_0\cos[\omega_0(t-2\Delta t)-k_0 z_1]$

where $z_1<0$, $\Delta z=c\Delta t$ and $E(z=z_1+\Delta z,t-\Delta t)-E_0\cos[\omega_0(t-2\Delta t)-k_0 z_1]$ represents the reflected wave. Letting $\Delta t\rightarrow 0$, the above expression is reduced to:

$$c\frac{\partial}{\partial z}E(z=z_1,t)-\frac{\partial}{\partial t}E(z=z_1,\omega_0 t)=2\omega_0 E_0\sin(\omega_0 t-k_0 z_1) \qquad (29)$$

On the exit side (right-hand side of Fig. 13) of the plasma slab, there is only a transmitted wave propagating toward right:

$$E(z=z_2,t)=E(z=z_2-\Delta z,t-\Delta t)$$

where $z_2>L$, $\Delta z=c\Delta t$. Letting $\Delta t\rightarrow 0$, the above expression is reduced to:

$$c\frac{\partial}{\partial z}E(z=z_2,t)+\frac{\partial}{\partial t}E(z=z_2,t)=0 \qquad (29')$$

Equations (29) and (29') are used to truncate the spatial extend of the numerical calculation.

The initial conditions of the problem are:

$$E(z,t=0)=E_0\cos(k_0 z)$$

$$\frac{\partial}{\partial t}E(z,t=0)=-\omega_0 E_0\sin(k_0 z) \qquad (30)$$

The boundary conditions (27) and (28), the initial conditions (30) together with the radiation conditions (29) and (29') supply the conditions for solving the wave equation (26). This model problem will be solved numerically in section 3 of this chapter.

To demonstrate the frequency up-shift, chamber experiments are performed and reported in the next section.

2. Experiments

Two experiments are performed to study frequency conversion of microwaves interacting with rapidly created plasmas. The first one considers the case that the maximum plasma frequency of the rapidly created plasma is less than the wave frequency. In the second experiment the maximum plasma frequency is much higher than the wave frequency.

A. The plasma frequency is less than the wave frequency

The experiment is conducted in a Plexiglas vacuum chamber of 2 foot cube filled with dry air, the same as the experiments discussed in the Chapter II. The plasma in the chamber is produced by two cross microwave beams split evenly from the output of the magnetron tube (which was used in the experiment reported in Chapter II.) The block diagram of this experimental arrangement is shown in Fig. 14.

Within the pressure range from 0.1 to a few torr, the microwave breakdown can occur with the available microwave power. The generated plasma layers are aligned in the direction perpendicular to the line bisecting the angle between the two intersecting beams (diagonal of the chamber). In the region near the aperture of the horns, the plasma clouds are produced since the electric field of a single beam in that region is already strong enough to breakdown the background gas. Fig. 15 is a photograph of the airglow emanating from the plasma layers and plasma clouds in side the chamber.

A pair of C-band horns are placed at the opposite sides of the chamber, and aligned in the direction parallel to the propagation direction of one of the microwave beams. One of them is used for injecting a cw source microwave into the chamber and the other one is used for receiving the test wave passing through the plasma clouds and layers. Whenever the breakdown microwave beams are turned on, the suddenly created

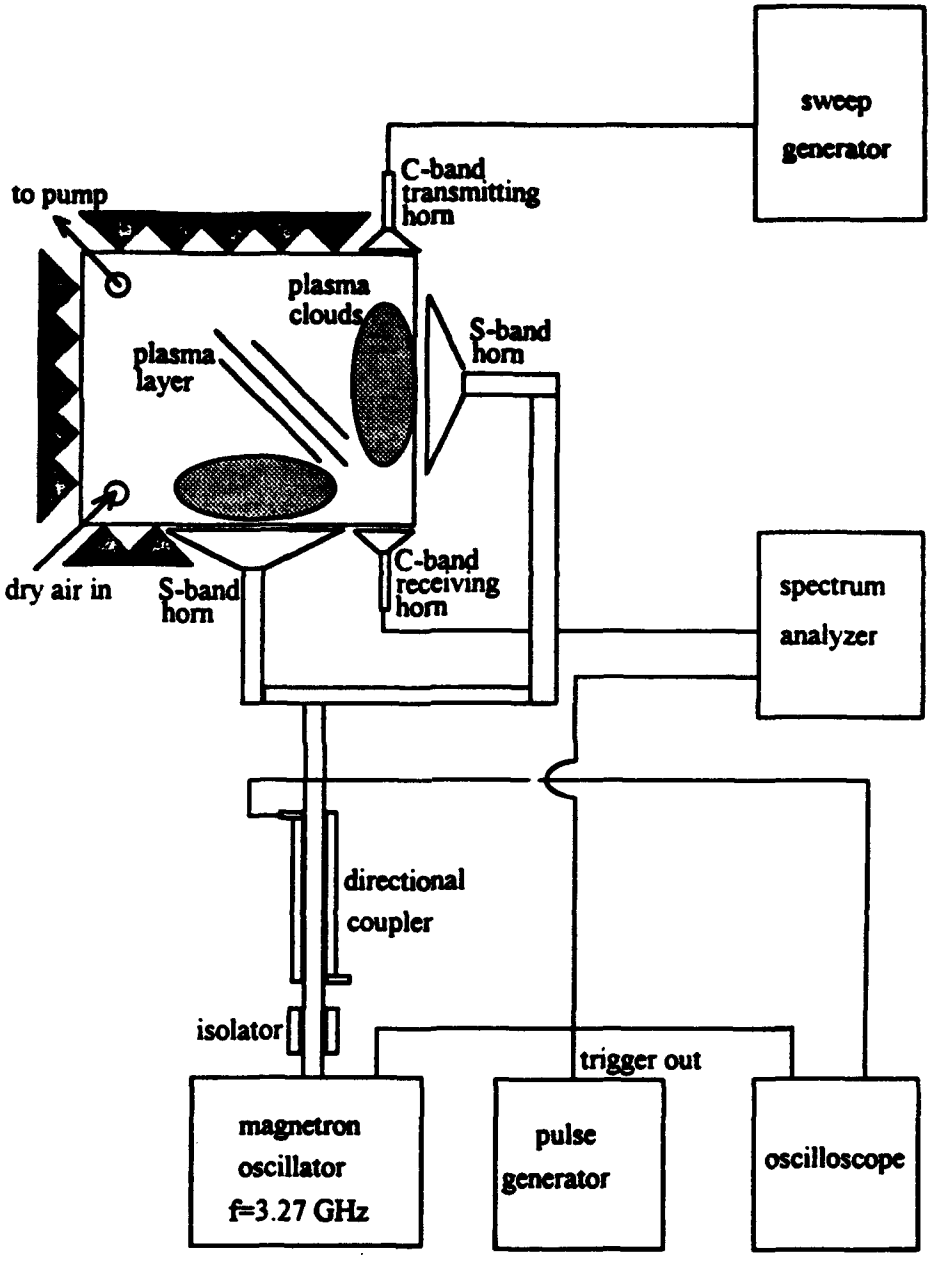

Fig. 14 Experimental setup for the experiment of cw wave propagating through a fast growing plasma. $\omega_{pe}<\omega_0$.

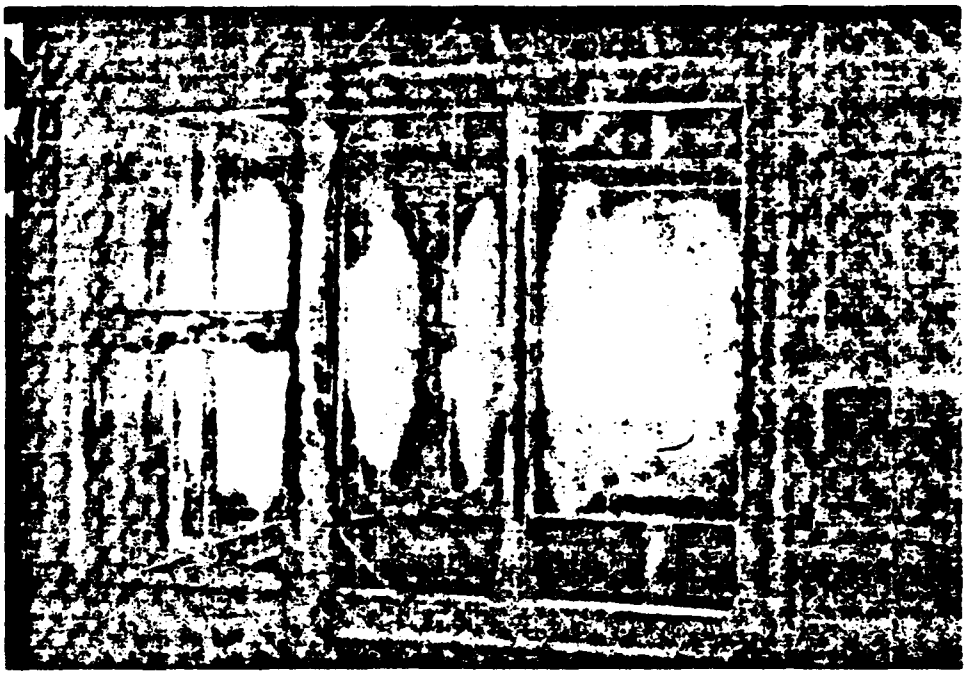

Fig. 15 A photograph of the air glow emanating from the plasma layers and plasma clouds.

plasma causes the sudden decrease of the dielectric constant of the background medium which forces the passing test wave to propagate at a higher phase velocity, and thus, to oscillate at a higher frequency. On the other hand, the plasma decays at a much slower rate during the off period of the microwave beams, and therefore, it does not affect the propagation of the source wave significantly ..Thus, the frequency of the test wave shifts back to the original frequency during this off period. In terms of the frequency characteristic, it suggests that the original cw wave be decomposed into two amplitude modulated waves (i.e., periodically on-off pulse trains) which appear alternatively and have the same modulation frequency as that of microwave beams. The first one of them has the same carrier frequency as the test wave and its off period is less than 1 μs. On the contrary, the period of the other periodic pulse is less than 1 μs, and its carrier frequency is up-shifted from that of the test wave.

In the experiment, a cw microwave of 4.833 GHz is used as the test wave. Since the 3.27 GHz microwave can only generate the maximum plasma density corresponding to the plasma frequency of 3.27 GHz, the maximum plasma frequency is less than the test wave frequency. The beam intensities of the ionization microwave pulses are adjusted to generate maximum plasma volume and also possibly to achieve the maximum ionization in the region passing by the cw test wave. The repetition rate of the breakdown microwave beams is chosen to be 35 Hz. The background dry air is about 300mtorr. The maximum plasma density (average over the volume) is about 0.5 of the cutoff density of the ionization microwave pulse. Therefore, the cw test wave is forced to be converted into two periodic pulses after interacting with the plasma generated by repetitive microwave discharge. The result is demonstrated by comparing the frequency spectrum of the transmitted source wave with that of the incident wave as shown in Fig. 16. The wave with a single spike at f=4.833 GHz represents the spectrum of the first periodic long pulse which is essentially the same as that of the cw source wave since the duty circle is so large and the repetition rate is so low (35 Hz). The remaining part of the spectrum has a

distribution of the form of $|\sin[2\pi(f-f_1)\tau/(f-f_1)]|^2$ which represents a frequency up-shifted [by 2.5 MHz, i.e., $(f_1-f_0)=\Delta f\sim 2.5$ MHz] microwave pulse of about $\tau=0.4$ μs duration and 35 Hz repetition rate. In this experiment, the maximum plasma density is always less than the cutoff density of the source wave, and the plasma growth rate is relatively small (so that only a small percentage of frequency up-shift is observed). The pulse length (0.4 μs) is mainly determined by the plasma growth period, instead of the transit time of the test wave passing through the chamber. The achievable up-shift is small because the density and growth rate of the plasma are limited by the frequency and power of the breakdown microwave beams. Though this experiment provides a clear demonstration of the feasibility of using the interaction with a repetitive fast gaseous discharge to convert a cw source wave into a frequency up-shifted periodic pulse, one has yet to show that large frequency up-shift is achievable for the purpose of practical applications. In order to do, an experiment with the maximum plasma frequency being much larger than the test wave frequency is performed.

B. The plasma frequency is greater than the wave frequency

The experiment is conducted by using a DC discharge to generate a fast growing dense plasma for frequency shifting purpose. The electrodes for the electrical discharge consist of a pair of parallel conducting plates placed inside a Plexiglas vacuum chamber. The electrode pair is also used to guide the incident wave. A Marx bank facility rated at 240 KV and 13 KJ maximum energy is used for the required fast generation of a dense plasma. In this experiment, the Marx bank is regulated by an internal impedance of 15Ω and only charged to about 100KV. The chamber is filled with dry air to about 1 torr pressure which is near the highest pressure allowed before getting into constricted arc discharge. The separation between the plates is about 15 cm leading to an open circuit average field strength of 6.6KV/cm which is much higher than the breakdown threshold

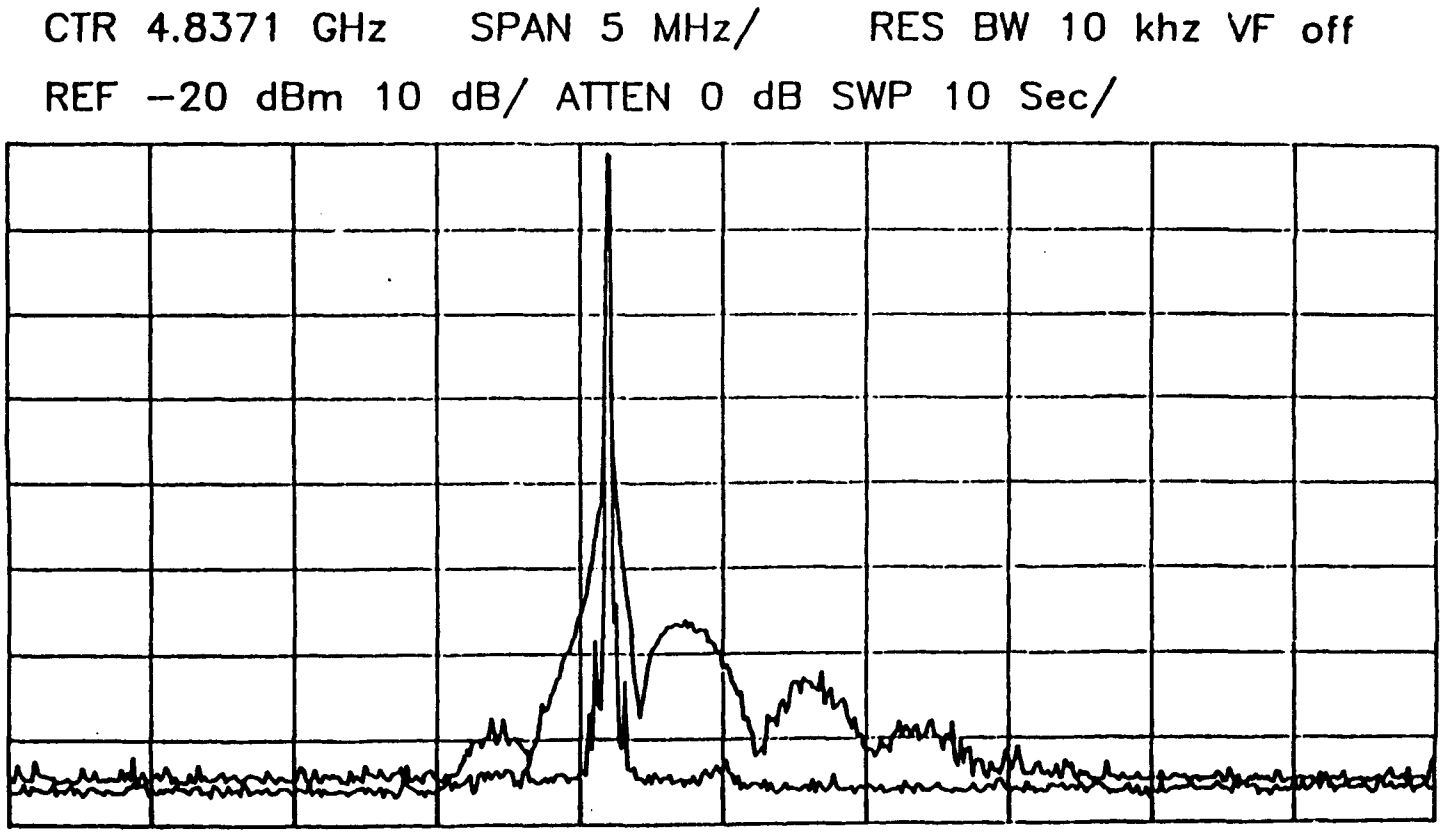

Fig. 16 The recorded spectra of the incident and transmitted wave. The one with a single spike at f=4.833 GHz is the spectrum of the incident source wave. The other one is the spectrum of the transmitted wave.

field of 40V/cm. After the gas breakdown caused by the applied high voltage, a dense plasma with reasonably uniform density distribution between the two parallel plates is generated, and the voltage across the electrodes drops considerably to slow down the ionization since the internal impedance of the Marx bank is fairly large compared to the impedance of the induced plasma between the parallel plate electrodes. Hence, the plasma growth procedure can be considered as two steps: first, at the beginning of the discharge almost all of the voltage on the Marx bank is applied to the electrodes and the ionization frequency is very high, so the electron plasma density grows very fast; then, after the electron plasma density reaches a certain level, the impedance between the electrodes drops to a low value comparing to the Marx bank internal impedance and most of the voltage on the Marx bank drops on the internal impedance, so the ionization frequency decreases. As a consequence, the electron plasma density grows much slower than that in the first stage. Eventually, when most of the energy stored in the Marx bank is released, the plasma starts to decay at a rate depending on the loss mechanisms which is very slow. A schematic of the complete experimental setup is presented in Fig. 17., in which the dimensions of the electrodes and the vacuum chamber are also indicated.

A cw source wave of 4.7GHz is injected into the chamber to propagate along the parallel plate waveguide. Without plasma generation the spectrum of the signal received at the other end of the chamber by a spectrum analyzer is a single spike at 4.7GHz. On the other hand, whenever the discharge takes place, the suddenly created plasma modifies the characteristics of the propagating wave, and different spectral components appear. The density of the generated plasma is measured indirectly in terms of the enhanced airglow, whose relationship with the actual plasma density is calibrated by the airglow corresponding to a microwave cutoff density, and measured in a separate experimental setup. Shown in Fig. 18 (a) is the spatial distribution of the peak intensity of the airglow emitting from a 1μs microwave pulse-induced plasma, whose peak near the entrance of the pulse adjusted by the microwave power to be about $10^{11}cm^{-3}$, is the cutoff density of

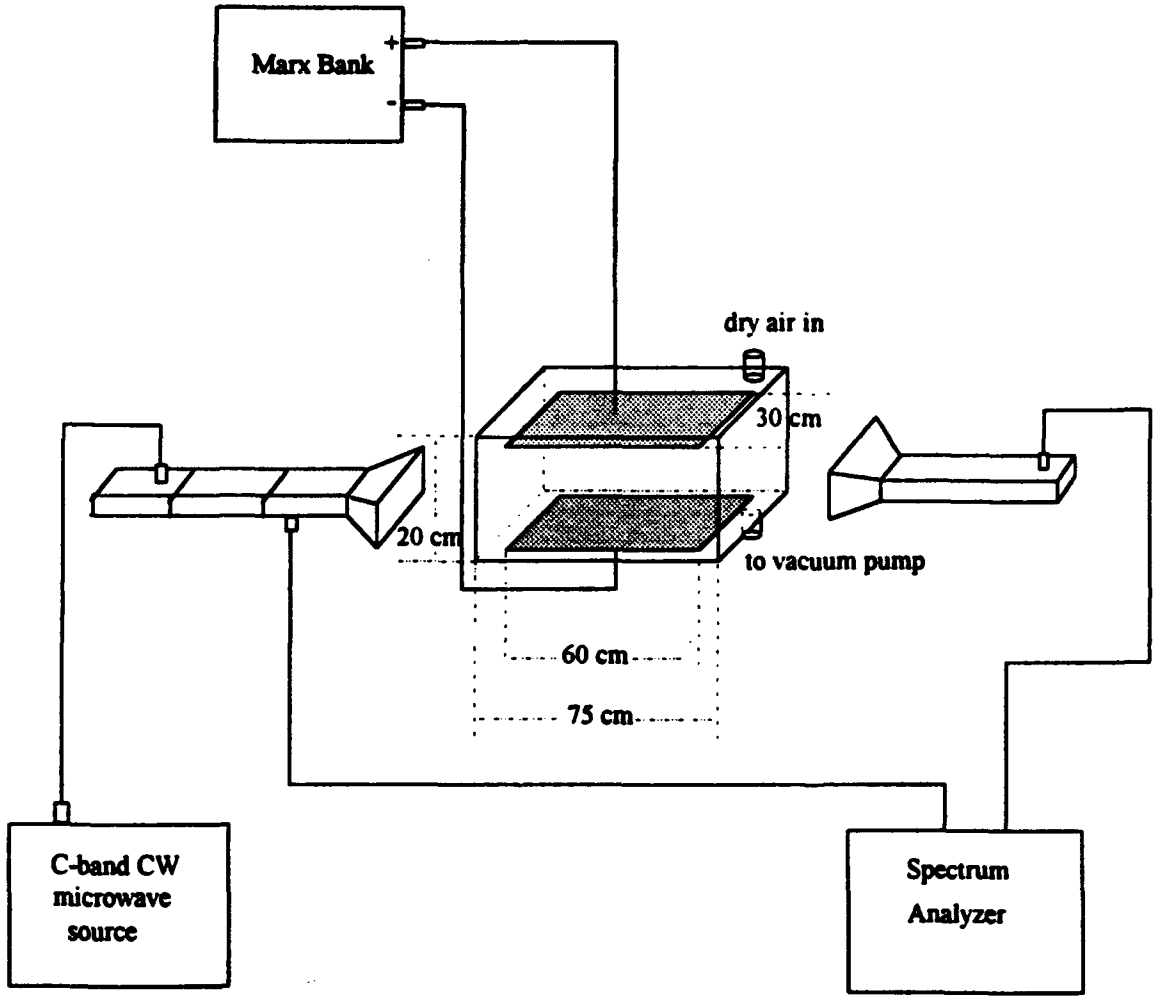

Fig. 17 The schematic diagram of the experimental setup for the experiment of cw wave propagating through a fast growing plasma slab with $\omega_{pe,max} >> \omega_0$.

the 3.27 GHz microwave. The temporal evolution of the intensity of the airglow of the DC discharge plasma is shown in Fig. 18 (b), which is compared with Fig. 18 (a) and indicates that the peak plasma density is about 8 times the cutoff density of the test microwave with frequency of 4.7GHz. In both systems, background air pressure is set at 1 torr. Since the plasma density is much higher than the cutoff density of the incident wave, the incident wave is blocked by the plasma from propagation through the chamber, and only the portion of the wave inside the chamber prior to the discharge can still propagate through the chamber. Thus, the transmitted signal is expected to be a pulse of about 2ns duration, i.e., the transit time of the test wave propagating through the chamber. Since the plasma is generated rapidly, it is also expected that the central frequency of the spectrum of the pulse will be up-shifted. Moreover, since the plasma density increases with finite growth rate, the pulse is expected to experience a time dependent frequency up-shift. Including all of the expected features, a frequency up-shifted and chirped 2ns pulse is expected to be generated by the interaction. Such a pulse is indeed observed in the experiment. The result of the experiment is demonstrated by its spectral distribution shown in Fig. 19. This spectrum is recorded by using the time sampling method. The spectrum analyzer measures a single frequency component of the output signal in each discharge. Each measured component represents a sampling value of the frequency spectrum of the transmitting signal at a given frequency. The spectrum of Fig. 19 is constructed from the data of more than 100 consecutive discharges. The peak line of 4.7GHz is the spectrum of the incident cw signal. The remaining lines are the sampling lines of the frequency spectrum of the chirped pulse. As seen, it is a broadband spectrum whose central frequency is up-shifted away from the original line of 4.7GHz. It is noted that the spectral distribution around 6.4GHz has a bandwidth about 500MHz and is asymmetric. It represents a 2ns chirped pulse whose pulse length is consistent with the transit time of the source wave propagating through the chamber as discussed before. The appearance of the other lines in Fig. 19 is believed to be attributed to the non-stationary

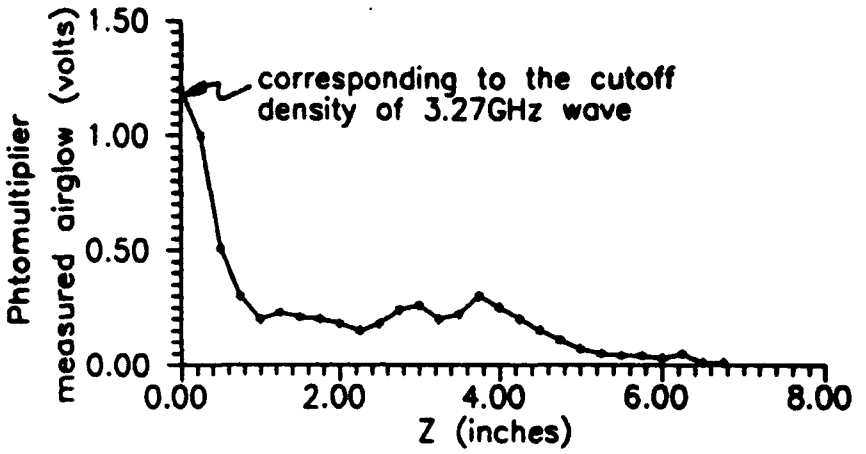

Fig. 18 (a) Spatial distribution of the peak airglow intensity emitting from an 1μs 3.27 GHz microwave pulse induced plasma

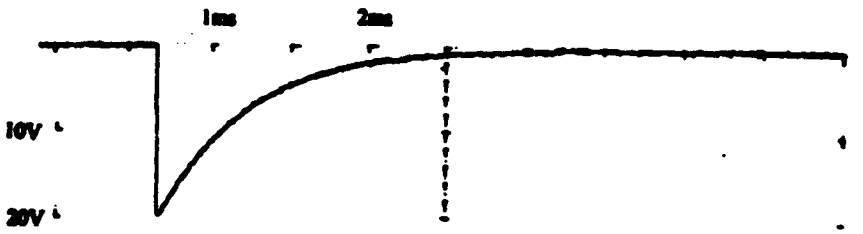

Fig. 18 (b) Temporal evolution of airglow intensity from the DC discharge plasma.

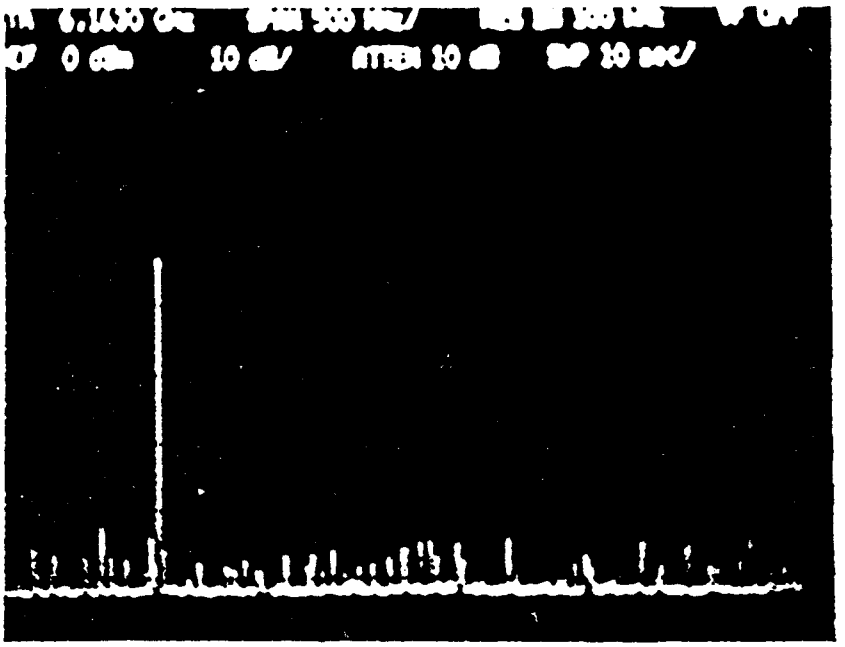

Fig. 19 The recorded spectra of the incident and transmitted wave. The one with a single spike at f=4.7 GHz is the spectrum of the incident source wave. The rest are the spectrum of the transmitted wave.

growth rate and decay rate of the plasma.

In next section , the numerical simulations are performed based on the theoretical model built in the first section.

3. Numerical simulation

For numerical analysis, the wave equation (26) is normalized into a dimensionless form. This is done by letting $\tau=\omega_0 t \rightarrow t$, $z'=\omega_0 z/c \rightarrow z$, $\bar{\nu}/\omega_0 \rightarrow \bar{\nu}$, $\alpha_1/\omega_0 \rightarrow \alpha$, $\omega_{pe}/\omega_0 \rightarrow \omega_{pe}$, and $E/E_0 \rightarrow E$, where E_0 is the amplitude of the incident cw wave, and substituting them into equation (26). The equation (26) can be rewritten as :

$$\frac{\partial^2}{\partial t^2}E-\frac{\partial^2}{\partial z^2}E+\omega_{pe}^2E=0 \qquad (31)$$

where

$\omega_{pe}^2(z,t)=u(t)g(z)\omega_{pe0}^2\exp[\alpha_1(t)t]$, $0<t<t_0$, while plasma density is rising.

$\omega_{pe}^2(z,t)=u(t)g(z)\omega_{pe0,max}^2\exp[-\alpha_2(t)t]$, $t>t_0$, while plasma density is decaying.

where ω_{pe0} and $\omega_{pe0,max}^2$ are the background plasma frequency and maximum plasma frequency respectively, t_0 is the ionization time interval.

The boundary conditions are:

$$E(z=0^-,t)=E(z=0^+,t) \text{ and } E(z=L^-,t)=E(z=L^+,t) \qquad (32)$$

and

$$\frac{\partial}{\partial z}E(z=0^-,t)=\frac{\partial}{\partial z}E(z=0^+,t) \text{ and } \frac{\partial}{\partial z}E(z=L^-,t)=\frac{\partial}{\partial z}E(z=L^+,t) \qquad (32')$$

The radiation conditions for truncations are

$$\frac{\partial}{\partial z}E(z=z_1,t)-\frac{\partial}{\partial t}E(z=z_1,t)=2\sin(t-z_1) \qquad z_1<0 \qquad (33)$$

and

$$\frac{\partial}{\partial z}E(z=z_2,t)+\frac{\partial}{\partial t}E(z=z_2,\omega_0 t)=0 \qquad z_2>L \qquad (33')$$

The initial conditions of the problem are

$$E(z,t=0)=\cos(z) \qquad (34)$$

and

$$\frac{\partial}{\partial t}E(z,t=0)=-\sin(z) \qquad (34')$$

Equation (31) subjected to the conditions (32), (32'), (33), (33'), (34) and (34') is solved numerically.

In simulating the experiment conducted in section 2A, the maximum plasma frequency is set to be 0.707×3.27 GHz =2.3 GHz, and the normalized maximum plasma frequency is 0.478 . The ionization time interval t_0 is chosen as 0.4 μs, which corresponds to the normalized value $t_0=1.2146\times10^4$. The normalized background plasma density is chosen as 10^{-5}. The plasma growth rate is assumed to be a constant and has a value that leads the growth of the plasma density from the background value to the maximum value over the ionization time t_0. Its normalized value is calculated as $\alpha_1=0.826\times10^{-3}$. The length of the plasma slab is about 24 cm (a slightly longer than the size of the horn transmitting the ionization beam), and its normalized value is L=26.29. The normalized

cw wavelength is $\lambda_0=2\pi$. Thus, $L/\lambda_0=4.186$. Shown in Fig. 20 is the spectrum of the transmitted wave obtained by the numerical simulation. One can see that the spectrum in Fig. 20 agrees well with the experimental result shown in Fig. 16.

To calculate the spectrum corresponding to the experimental result presented in Fig. 19, the maximum plasma density is set to be $8\omega_0^2$. Thus, the normalized maximum plasma density is 8. The background plasma density is chosen as 10^{-10} (normalized). Since the time period between each discharge is very long (more than 3 min), the plasma density decays to its original background density before next discharge. The plasma growth rate is modeled by two values, $\alpha_1=2.36\times10^{10}$ sec^{-1} for $t<0.68$ ns (normalized value $\alpha_1=4.13$); and $\alpha_1=2.95\times10^{7}$ sec^{-1} for $t>0.68$ ns (normalized value $\alpha_1=9.99\times10^{-4}$). The modeling of the growth rate by two values is based on the understanding that the discharging voltage provided by the Marx bank decreases in time. The initial α_1 value for $t<0.68$ ns is chosen to agree with the average ionization rate of the dry air during the beginning 0.68 ns time interval. The maximum discharge current of the Marx bank regulated by its internal impedance is taken into account to determine the time of 0.68 ns. The second α_1 value for $t>0.68$ ns is chosen as a variable parameter. The length of the plasma slab is about 60 cm (the length of the parallel plate electrodes), its normalized value is $L=63.92$. The normalized cw wavelength $\lambda_0=2\pi$. Thus, $L/\lambda_0=10.18$. Presented in Fig. 21 is the spectrum of the numerical simulation, which is similar to the experimental result shown in Fig. 19. The resemblance between the spectra of Fig. 20 and Fig. 16, as well as between those of Fig. 21 and Fig. 19, suggests that a vital model has been developed and the frequency shift mechanism has been validated. The model can be used to guide the future experiments.

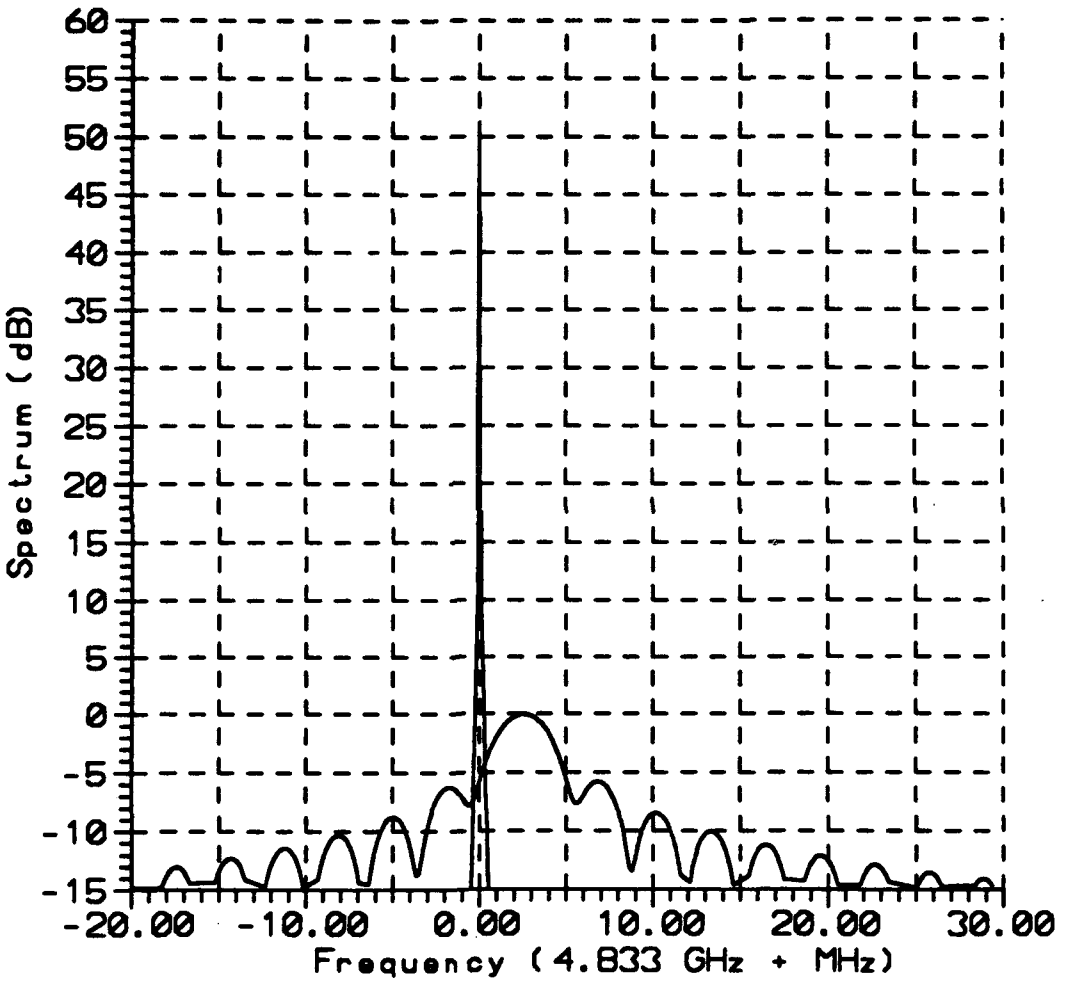

Fig. 20 The numerical simulation spectra of the incident and transmitted wave. The one with a single spike at f=0 MHz represents the spectrum of the incident source wave. The other one is the spectrum of the transmitted wave.

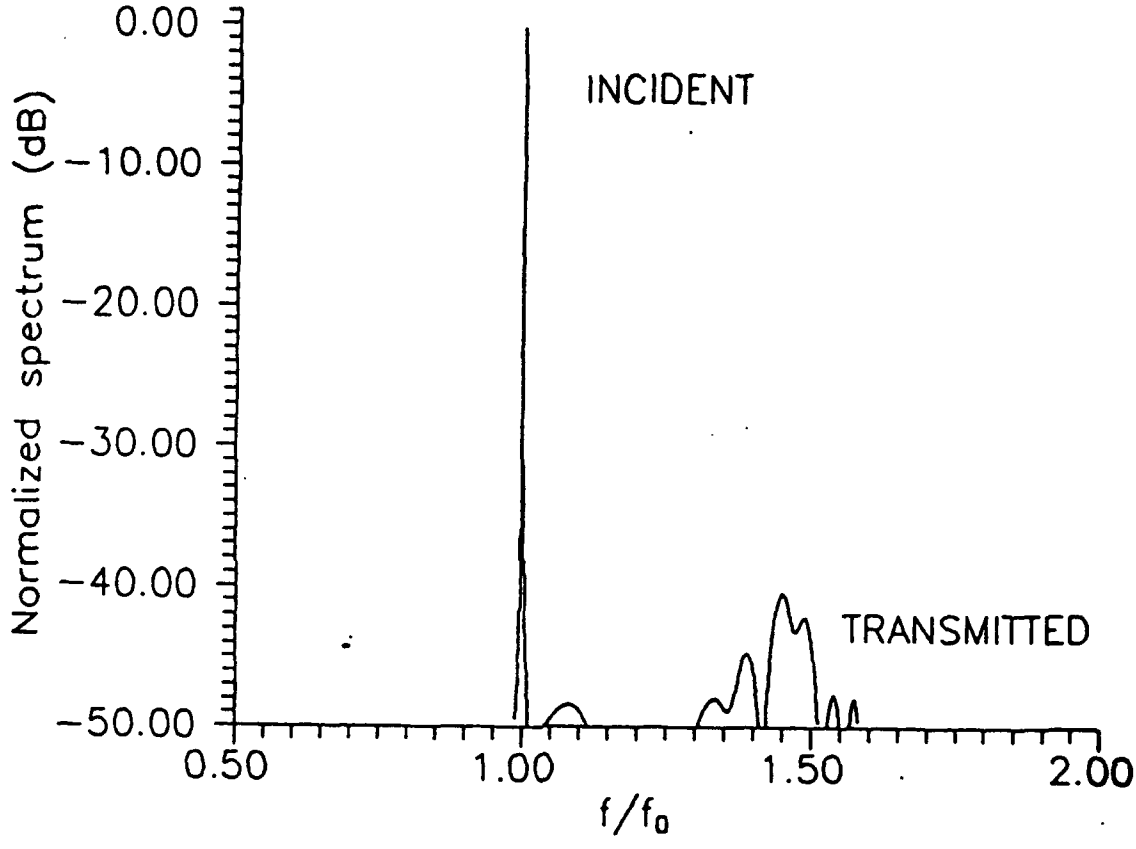

Fig. 21 The numerical simulation spectra of the incident and transmitted wave. The one with a single spike at $f/f_0=1$ represents the spectrum of the incident source wave. The rest are the spectrum of the transmitted wave.

4. Summary

In this chapter, the study of electromagnetic wave propagating in a rapidly created plasma is reported. The problem is cast as a cw wave propagating through a fast growing plasma slab, an initial value problem mixed with the boundary effect. A theoretical model is developed. Experiments are performed for different maximum plasma densities (i.e., Max. ω_{pe} is greater and less than the wave frequency ω_0). Frequency up-shifts are observed in both situations. Numerical simulations based on the developed model are also performed to compare with the experimental results. Good agreement of the comparison suggests that the theoretical model is vital. It is noted when the maximum plasma frequency is less than the wave frequency, there is no cutoff to the wave propagation. The wave will continuously propagate through the time varying plasma slab, and its frequency is up-shifted during the period of plasma growth. In this case the frequency up-shifted wave component is a pulse. The width of the pulse depends on the rising period of the plasma density, and the amount of frequency up-shift over the original carrier frequency depends on the growth rate of the plasma density. By generating the rapidly growth plasma periodically, one can convert a cw wave into two pulse trains. One has an up-shifted carrier frequency and plasma growth period duration, and the other one has the original cw wave frequency as carrier frequency, and the duration of it is basically the plasma off time (plus the plasma decaying time, to be precise). The repetition rate of these pulse trains is the same as the repetition rate of rapidly created plasma. However, when the maximum plasma frequency is much greater than the incident wave frequency, the plasma frequency quickly exceeds the incident wave frequency, and the incident wave is cutoff. Only the wave which is already inside the plasma slab can experience the rise of the plasma frequency. Hence, the transmitted signal is a pulse whose duration determined by the length of the plasma slab (The transit time of a wave through the plasma slab, here the time needed for plasma frequency to exceed the wave frequency is assumed

negligible). The amount of frequency up-shift of the transmitted signal (pulse) depends on the growth rate of the plasma frequency again.

The frequency up-conversion efficiency is estimated as follows. In the experiment discussed in section 2A, the incident cw wave bandwidth is 100 KHz, the spectral bandwidth of the transmitted up-shift pulse is increased to about 3 MHz, but its amplitude is about 55 dB down. Thus, the conversion efficiency is about -40 dB or 0.01%, which is quite low. In the second experiment reported in the section 2B, the incident cw wave has also a bandwidth of 100 KHz, however, the transmitted up-shift pulse has a bandwidth of about 500 MHz and only about 40dB down in amplitude. Thus, the conversion efficiency in this case is estimated to be -3 dB or 50%, which is quite high. The large difference between these two conversion efficiencies is due to the difference in the characters of the plasmas involved in the two experiments. The plasma in the experiment of 2B has a much faster growth rate and higher plasma density than that in the experiment of 2A, thus, the conversion efficiency is much higher.

Chapter IV
Conclusion

In this work, the electromagnetic wave propagating in a fast growing plasma is studied experimentally and numerically. Theoretical models are developed to assist the numerical simulations. The plasma media involved in the study is classified into two categories, (1) the plasma density varies both temporally and spatially; (2) the plasma density is a function of time only. It is shown that the results of the numerical simulations based on the theoretical models agree well with those of the experiments. The agreement validates the developed theoretical models which can be used to guide and understand the future experiments on high power microwave pulse propagation and the future experiments for developing practical plasma devices.

The present study shows that the spectrum of a microwave will be modified while propagating through a fast growing plasma. In the case of high power microwave pulse propagating in a self-generated plasma, the carrier frequency of the pulse is up-shifted only when the power of the microwave pulse is just slightly above the breakdown threshold of the background gas (<15%). In this case, the pulse shape is not distorted significantly. However, when the power of the pulse is further increased (30% over the breakdown threshold), both frequency up-shift and down-shift occurs, i.e. the spectrum of the pulse breaks up into up-shifted and down-shifted peaks. The amounts of the up-shift and down-shift frequency are shown to be comparable in the experimental condition of the present work, it suggests that an understanding of the frequency down-shift phenomenon is needed. Computer experiments based on the developed theoretical model are then performed to identify the mechanism causing the frequency downshift. It is shown that the effective collision loss of the pulse in the self-generated plasma causes the frequency downshift. In order to use the frequency up-conversion process to avoid the cutoff reflection of a high power microwave pulse by the self-generated plasma, one has to be

sure that the effective collision frequency of the plasma is low comparing to the plasma frequency of the self-generated plasma. Otherwise, the effective loss process of the microwave pulse will cause part of the frequency spectrum of the pulse to down-shift, and tail erosion of the pulse will be further enhanced. It is then most of the pulse energy will be eroded and the remaining leading edge can not deliver enough energy for the purpose of interest.

The present work also shows that in the case of a wave propagating through a fast growing uniform (over the space) plasma, the frequency of the wave is up-shifted. When the maximum plasma density (generated by two cross beams of microwave pulses) does not exceed the cutoff density of the wave, the wave is converted into a frequency chirped pulse train. The width of the chirped pulse depends on the plasma growing period, the frequency depends on the growth rate of plasma density, and the repetition rate depends on the repetition rate of the generated plasma. The present work shows that a pulse train is generated with the width of 0.4 μs, the repetition rate of 35 Hz and the chirped frequency of 2.5 MHz higher than the original cw wave frequency. When the maximum plasma density (generated by dc Marx bank discharge) is much higher than the wave cutoff density, the transmitted wave is a frequency up-shifted short pulse. The duration of the pulse is determined by the wave transit time through the plasma volume, and the carrier frequency is determined by the growth rate of the plasma density. The present work shows that a short pulse is generated with a width of 2 ns and an up-shifted frequency of 40% higher than that of the original cw wave. The frequency up-shift process can be used to extend the usage of the existing microwave source or generated ultra wideband short pulse from a cw wave. Research on implementation of this process in microwave devices is ongoing.

References:

1. E. Yablonovitch, "Spectral Broadening in the Light Transmitted through a Rapidly Growing Plasma", Phys. Rev. Lett., Vol. 31, No. 14, pp.877-879, 1973.
2. E. Yablonovitch, "Self-Phase Modulation of Light in a Laser-Breakdown Plasma", Phys. Rev. Lett., Vol. 32, No. 20, pp.1101-1104, 1973.
3. C.L. Jiang, "Wave Propagation and Dipole Radiation in a Suddenly Created Plasma", IEEE Trans., Antenna and Propagation, AP-23, No. 1, pp.83-90, 1975.
4. S.C. Wilks, J.M. Dawson, and W.B. Mori, "Frequency Up-conversion of Electromagnetic Radiation with Use of an Overdense Plasma", Phys. Rev. Lett., Vol. 61, No. 3, pp337-340, 1988.
5. S.P. Kuo, "Frequency Up-conversion of Microwave Pulse in a rapidly Growing Plasma", Phys. Rev. Lett., Vol. 65, No. 8, pp.1000-1003, 1990.
6. C. Joshi, C.E. Clayton, K. Marsh, D.B. Hopkins, A. Sessler, and D. Whittum, "Demonstration of the Frequency Up-shifting of Microwave Radiation by Rapid Plasma", IEEE. Trans. Plasma Science, Vol. 18, pp.814-818, 1990.
7. M. Rader, and I. Alexeff, "Frequency Modulation of free Space R.F. Signals", IEEE Int'l Conf., 1A2, 1Ch3037-9, Williamsburg, VA, June, 1991.
8. R.L. Salvage, Jr., C. Joshi, and W.B. Mori, "Frequency Upconversion of Electromagnetic Radiation upon Transmission into an Ionization Front", Phys. Rev. Lett., Vol. 68, pp.946-949, 1992.
9. S.P. Kuo, A. Ren, and J. Huang, "Generation of a Frequency Chirped Pulse Using Phase Velocity Transitions in a Rapidly Created Plasma", Int'l Conf. on Ultral-Wideband, Short-Pulse Electromagnetics, edited by H. Bertoni et al., Plenum Press, pp.129-136, 1993.
10. S.P. Kuo, and A. Ren, "Experimental Study of Wave Propagation through a Rapidly Created Plasma", IEEE. Trans. Plasma Science, Vol. 21, No. 1, pp.53-56, 1993.

11. M.S. Rader, "Frequency Modification of R.F. Signals Using an Ionized Gas", A Dissertation for Ph. D degree, The university of Tennesse, Knoxiville, May, 1991.

12. W.M. Bollen, C.L. Yee, A.W.Ali, M.J. Nagurney, and M.E. Read, "High Power Microwave Energy Coupling to Nitrogen during Breakdown", J. Appl. Phys. vol. 54, No. 1, pp.101- , 1983.

13. Wee Woo and J.S. DeGroot, "Microwave Absorption and Plasma Heating due to Microwave Breakdown in the Atmosphere", Phys. Fluids 27, No. 2, pp.475-487, 1984.

14. J.H. Yee, R.A. Alvarez, D.J. Mayhall, D.P. Byrne, and J. DeGroot, "Theory of Intense Electromagnetic Pulse Propagation through the Atmosphere", Phys. Fluids 29, No. 4, pp.1238-1244, 1986.

15. M.J. Mulbrandon, J. Chen, P.J. Palmadesso, C.A. Sullivan, and A.M. Ali, "A Numerical Solution of the Boltzmann Equation for High-powered Short Pulse Microwave Breakdown in Nitrogen", Phys. Fluids B 1, No. 12, pp2507-2515, 1989.

16. S.P. Kuo, and Y.S. Zhang, "Bragg Scattering of Electromagnetic Waves by Microwave-Produced Plasma Layers", Phys. Fluids B 2, No. 3, pp.667-673, 1990.

17. S.P. Kuo, Y.S. Zhang, and Paul Kossey, "Propagation of High-power Microwave Pulses in Air Breakdown Environment", J. Appl. Phys. Vol. 67, No. 6, pp.2762-2766, 1990.

18. S.P. Kuo, and Y.S. Zhang, "A Theoretical Model for Intense Microwave Pulse Propagation in an Air Breakdown Environment", Phys. Fluids B 3, No. 10, pp2906-2912, 1991.

19. J.H. Yee, D.J. Mayhall, G.E. Sieger, and R.A. Alvares, "Propagation of Intense Microwave Pulse in Air and in a Waveguide", IEEE. Trans. Antennas and Propagation, AP-39, pp.1421-1429, 1991.

20. V.B. Gildenburg, V.A. Krupnov, and V.E. Semenov, "Frequency Autoconversion and Reflectionless Propagation of a Powerful Electromagnetic Pulse in an ionizing medium", Sov. Tech. Phys. Lett. 14, pp.783, 1988.

21. S.P. Kuo, Y.S. Zhang, and A. Ren, "Observation of Frequency Up-conversion in the Propagation of a High-power Microwave Pulse in a Self-generated Plasma", Phys. Lett. A. 150, pp.92-96, 1990

22. S.P. Kuo, and A. Ren, "Frequency Up-conversion of a High Power Microwave Pulse Propagating in a Self-generated Plasma", J. Appl. Phys. 71, No. 11, pp.5376-5380, 1992.

23. Yu. A. Lupan, "Refined Theory for a RF Discharge in Air", Sov. Phys. Tech. Phys. Vol. 21, No. 11, pp1367-1370, 1976.

24. A.V. Gurevich, "Ionizaton of the Lower Ionospher under the Effect of Strong Radio Pulses", Geomag. Aeronom. 19, No. 4, pp.428-432, 1979.

25. F. F. Chen, "Plasma Diagnostic Techniques", Edited by R.H. Huddlestone and S.L. Leonard, (Academic Press, New York), Chapter 4 "Electric Probe", pp.113-200.

26. A. C. Hindmarsh, "LSODE and LSODI, two initial value ordinary differential equation solvers", ACM-SIGNUM newsletter, Vol. 15, No. 4, pp.10-11, 1980.

27. L. R. Petzold, "Automatic Selection of Mathods for Solving Stiff and Nonstiff Systems of Ordinary Differential Equations", Sandia National Lab. Report, SAND80-8230, Sept., 1980.

28. K. L. Hiebert and L. F. Shampine, "Implicitly Defined Output Points for Solutions of ODE's", Sandia National Lab. Report, SAND80-0180, Feb., 1980.